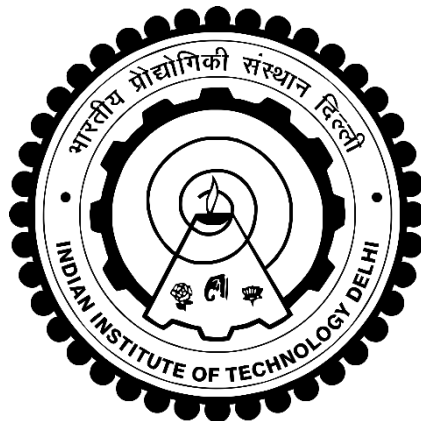


**DESIGN AND CONTROL OF PERMANENT MAGNET
SYNCHRONOUS MOTOR DRIVES FOR STANDALONE AND
GRID INTERFACED SOLAR WATER PUMPING SYSTEMS**

MOHD. KASHIF



**ELECTRICAL ENGINEERING DEPARTMENT
INDIAN INSTITUTE OF TECHNOLOGY DELHI
HAUZ KHAS, NEW DELHI-110016, INDIA
MAY, 2023**

© Indian Institute of Technology Delhi (IITD), New Delhi, 2023

**DESIGN AND CONTROL OF PERMANENT MAGNET
SYNCHRONOUS MOTOR DRIVES FOR STANDALONE AND
GRID INTERFACED SOLAR WATER PUMPING SYSTEMS**

by

MOHD. KASHIF

Submitted
in fulfilment of the requirements of the degree of Doctor of Philosophy
to the



**ELECTRICAL ENGINEERING DEPARTMENT
INDIAN INSTITUTE OF TECHNOLOGY DELHI
HAUZ KHAS, NEW DELHI-110016, INDIA
MAY, 2023**

CERTIFICATE

It is certified that the thesis entitled “**Design and Control of Permanent Motor Synchronous Motor Drives for Standalone and Grid Interfaced Solar Water Pumping System,**” being submitted by **Mr. Mohd. Kashif** for award of the degree of **Doctor of Philosophy** in the Department of Electrical Engineering, Indian Institute of Technology Delhi, is a record of the student work carried out by him under my supervision and guidance. The matter embodied in this thesis has not been submitted for award of any other degree or diploma.

(Prof. Bhim Singh)
Electrical Engineering Department
Indian Institute of Technology Delhi
Hauz Khas, New Delhi-110016, India

Dated:

ACKNOWLEDGEMENTS

I wish to express my deepest gratitude and indebtedness to **Prof. Bhim Singh** for providing me guidance and constant supervision to carry out the Ph.D. work. Working under him has been a wonderful experience, which has provided a deep insight to the world of research. Determination, dedication, innovativeness, resourcefulness and discipline of **Prof. Bhim Singh** have been the inspiration for me to complete this work. I truly appreciate and value his esteemed guidance and encouragement from the beginning to the end of this thesis. I am indebted to him for having helped me shape the problem and providing insights towards the solution. His consistent encouragement, continuous monitoring and commitments to excellence have always motivated me to improve my work and use the best of my capabilities. Due to his blessing, I have earned various experiences, other than research, which will help me throughout my life.

My sincere thanks and deep gratitude are to **Prof. B. K. Panigrahi, Prof. G. Bhuvanewari, Dr. Anandarup Das** and **Dr. Ashu Verma**, all SRC members for their valuable guidance and consistent support during my research work.

I wish to convey my sincere thanks to **Prof. Bhim Singh, Prof. M. L. Kothari, Dr. Anandarup Das, Prof. I. N. Kar** for their valuable inputs during my course work, which made the foundation for my research work. I am grateful to IIT Delhi for providing me the research facilities. I would wish to express my sincere gratitude to **Prof. Bhim Singh, Prof. G. Bhuvanewari** and **Dr. Anandarup Das**, as Prof. in-charge of PG Machines Lab, for providing me immense facilities to perform experimental work. Thanks are due to Sh. Srichand, Sh. Puran Singh, Sh. Amit Kumar, Sh. Jitender Kumar, Sh. Anurag Singh, Sh. Rahul Diwakar of PG Machines Lab, UG Machines Lab and Power Electronics Lab., IIT Delhi for providing me the facilities and assistance during this work.

I would like to use this opportunity to thank Dr. Rajan, Dr. Ikhtlaq, Dr. Shadab, Dr. Nishant, and Dr. Chinmay who have helped me in deciding my research goal and helped me sincerely in the initial phase of my journey in Ph. D. It would be incomplete without thanking Dr. Nishant, Dr. Sachin, Dr. Aniket, Dr. Anshul, Dr. Shadab, Dr. Piyush and Dr. Radha without whose support it would have been very difficult to complete this research work. I would like to thank Dr. Shreejith, Dr. Anshul, Dr. Shailendra, Dr. Saurabh, Dr. Anajnee, Dr. Piyush, Dr. Priyank, Dr. Srinivas, Dr. Nidhi, Dr. Seema, Dr. Amresh Dr. Anjeet for their constant support in each and every moment and making the lab environment very calm and tranquil. Mr. Sambasivaiah, Ms. Farheen, Dr. Rohini, Dr. Pavitra, Dr. Utkarsh, Dr. Shubhra, Mr. Munesh and Mr. Gurmeet have been very supportive and I would like to thank them for being very good to me. My sincere thanks goes to Mr. Aryadip, Mr. Amarnath, Ms. Hina, Ms. Rashmi, Mr. Jitendra, Mr. Utsav, Ms. Yashi, Mr. Sudip, Mr. Sandeep, Mr. Gaurav, Mr. Bilal, Ms. Shalvi, Mr. Saran, Mr. Sayandev, Mr. Vivek, Mr. Praneeth, Mr. Priyvratt, Mr. Rahul, Mr. Sharan, Mr. Deepak, Mr. Shivam, Ms. Kousalya, Ms. Chandrakala, Mr. Rohit, Mr. Arjun, Mr. Sumit and all PG Machines laboratory group for their valuable support. I would also like to thank Mr. Yatindra, Mr. Satish, Mr. Narendra, Mr. Sandeep, Mr. Muresh and all other Electrical Engineering Department Office staff for being supportive throughout. I am likewise thankful to those who have directly or indirectly helped me to finish my dissertation study.

Moreover, I would like to thank **Ministry of Education (Formerly, Ministry of Human Resource Development), Government of India** and **Shakti Pumps (India) Ltd.** for funding this research work under UAY (Ucchatar Avishkar Yojana) project entitled Design and Development of Solar PV Based Super-Efficient Agricultural Pumps and Hybrid Multidimensional Inverters with grant number RP03222.

I would like to convey my unbounded love and thank to my father **Mr. Mohd. Idrees** and my mother **Ms. Aysha Begum** for showering their blessings on me. I would like to thank my wife

Ms. Zakiya for her forbearance, sacrifices, emotional and motivational support. I would like to convey my unbounded love to my son **Mr. Mohammad Ibrahim**, the apple of my eye. Moreover, I would like to thank my sisters **Ms. Gulistan** and **Ms. Gulfishan**, brothers **Mr. Mohd. Naushad**, **Mr. Mohd. Amjad**, **Mr. Humayoun**, and other family members and loving friends **Dr. Rafeeq Ahmad** and **Dr. Ahmad Riyaz** for giving me the inner strength and wholeheartedly support. Their trust in my capabilities had been a key factor to all my achievements.

At last, I am beholden to Almighty for His blessings to help me to raise my academic level to this stage. I pray for His benediction in my future endeavors. May His blessings be showered on me for strength, wisdom and determination to achieve in future.

Date: May 09th, 2023



Mohd. Kashif

ABSTRACT

Due to worldwide acceptance of net zero carbon emission policy and the subsequent necessity to minimize carbon footprints of energy infrastructure, there is an accelerated growth of solar photovoltaic (PV) array fed systems for several crucial applications like solar water pumping. The domains like irrigation, residential/commercial buildings, forest conservation, livestock, aquaculture and others are the potential beneficiary of solar water pumping systems. Besides, the declining cost of PV technology and the availability of low-cost digital signal processors have increased the number of installations of PV array fed water pumping systems. Meanwhile, permanent magnet synchronous motor (PMSM) has emerged as a potential candidate for driving solar water pumping systems due to its advantages like higher efficiency, higher torque density and unity power factor operation over induction motors. In this research work, various configurations of PMSM drive suitable for solar water pumping system.

In developed configurations of PMSM, the reverse-saliency is realized through introduction of flux barriers along q-axis in rotor to minimize permanent magnet demagnetization risk. While the developed topologies of PMSM operated solar water pumping system are broadly classified into standalone and grid interfaced systems. The PV array and battery energy storage (BES) are the two energy sources for standalone system. For such systems, a bidirectional power flow controller is developed for controlling battery power based on weather conditions. This enables delivery of constant water discharge for intermittent irradiation, thereby increasing utilization of the system. Whereas, the grid is available as another energy source in addition to PV array and BES for grid-interfaced system. Such a configuration facilitates on-demand water pumping irrespective of availability of irradiation. For this system, the fundamental component of grid voltage is extracted by using presented frequency locked loop (FLL). This enables the smooth operation of system even under abnormal grid conditions as the power quality at grid terminals is maintained in accordance to the IEEE-519 standard. Besides, a synchronization unit is added to the grid interfaced system for seamless synchronization of water pumping system with grid. For this purpose, the presented FLL based synchronizing controls are developed. Such a unit facilitates interconnection and interoperability between water pumping system and grid so that these two units work effectively, which thereby satisfies the IEEE 1547-2018 updated standard. Besides, mechanical position sensor is eliminated from PMSM drive by using presented rotor flux observer, which estimates speed and rotor position. The estimated speed and rotor position are then used for implementing field-oriented control of PMSM drive. The elimination of position sensor reduces cost and increases reliability of the solar water pumping system. Even

a provision to supply power to local-loads of the system such as pressure boosters, cooling fans, lighting load, fan-load and others is included into the system. Such a load is necessary and unavoidable as it represents the auxiliary components of solar water pumping system, which are necessary for smooth operation of the system.

The performance of the presented configurations of solar water pumping system and the associated control techniques is analyzed by performing simulation on MATLAB/Simulink platform. Several simulation results are acquired and reported for each topology during starting, steady-state and dynamics under practical operating scenarios. Besides, an experimental validation of all the presented topologies is carried out on the laboratory prototype of the system, and the associated test results are reported.

संक्षेप

शून्य कार्बन उत्सर्जन नीति की विश्वव्यापी स्वीकृति और ऊर्जा अवसंरचना के कार्बन फुटप्रिंट्स को कम करने की आवश्यकता के कारण, सौर जल पंपिंग जैसे कई महत्वपूर्ण अनुप्रयोगों के लिए सौर फोटोवोल्टिक (पीवी) सरणी फेड सिस्टम की त्वरित वृद्धि हुई है। सिंचाई, आवासीय/वाणिज्यिक भवनों, वन संरक्षण, पशुधन, जलीय कृषि और अन्य जैसे डोमेन सौर जल पंपिंग प्रणालियों के संभावित लाभार्थी हैं। इसके अलावा, पीवी तकनीक की घटती लागत और कम लागत वाले डिजिटल सिग्नल प्रोसेसर की उपलब्धता ने पीवी ऐरे फेड वॉटर पंपिंग सिस्टम की स्थापनाओं की संख्या में वृद्धि की है। इस बीच, स्थायी चुंबक तुल्यकालिक मोटर (PMSM) उच्च दक्षता, उच्च टोक़ घनत्व और प्रेरण मोटर्स पर एकता शक्ति कारक संचालन जैसे लाभों के कारण सौर जल पंपिंग सिस्टम को चलाने के लिए एक संभावित उम्मीदवार के रूप में उभरा है। इस शोध कार्य में पीएमएसएम ड्राइव के विभिन्न विन्यास सौर जल पंपिंग प्रणाली के लिए उपयुक्त हैं।

पीएमएसएम के विकसित विन्यास में, स्थायी चुंबक विचुंबकीकरण जोखिम को कम करने के लिए रोटर में क्यू-अक्ष के साथ फ्लक्स बैरियर की शुरूआत के माध्यम से रिवर्स-सलियेन्सी को महसूस किया जाता है। जबकि पीएमएसएम संचालित सौर जल पंपिंग प्रणाली की विकसित टोपोलॉजी को मोटे तौर पर स्टैंडअलोन और ग्रिड इंटरफेस सिस्टम में वर्गीकृत किया गया है। पीवी सरणी और बैटरी ऊर्जा भंडारण (बीईएस) स्टैंडअलोन सिस्टम के लिए दो ऊर्जा स्रोत हैं। ऐसी प्रणालियों के लिए, मौसम की स्थिति के आधार पर बैटरी पावर को नियंत्रित करने के लिए एक द्विदिश शक्ति प्रवाह नियंत्रक विकसित किया जाता है। यह आंतरायिक विकिरण के लिए निरंतर जल निर्वहन को सक्षम बनाता है, जिससे सिस्टम का उपयोग बढ़ता है। जबकि, ग्रिड-इंटरफेस सिस्टम के लिए पीवी सरणी और बीईएस के अतिरिक्त ग्रिड एक अन्य ऊर्जा स्रोत के रूप में उपलब्ध है। इस तरह का विन्यास विकिरण की उपलब्धता के बावजूद ऑन-डिमांड पानी पंपिंग की सुविधा देता है। इस प्रणाली के लिए, प्रस्तुत फ्रीक्वेंसी लॉक लूप (FLL) का उपयोग करके ग्रिड वोल्टेज के मूलभूत घटक को निकाला जाता है। यह असामान्य ग्रिड परिस्थितियों में भी सिस्टम के सुचारू संचालन को सक्षम बनाता है क्योंकि ग्रिड टर्मिनलों पर बिजली की गुणवत्ता IEEE-519 मानक के अनुसार बनाए रखी जाती है। इसके अलावा, ग्रिड के साथ जल पंपिंग प्रणाली के निर्बाध तुल्यकालन के लिए ग्रिड इंटरफेस प्रणाली में एक तुल्यकालन इकाई जोड़ी जाती है। इस प्रयोजन के लिए, प्रस्तुत FLL आधारित तुल्यकालन नियंत्रण विकसित किए गए हैं। ऐसी इकाई जल पंपिंग प्रणाली और ग्रिड के बीच अंतर्संबंध और अंतर्संचालनीयता की सुविधा प्रदान करती है ताकि ये दोनों इकाइयाँ प्रभावी ढंग से काम करें, जिससे IEEE 1547-2018 अद्यतन मानक को पूरा किया जा सके।

इसके अलावा, प्रस्तुत रोटर फ्लक्स ऑब्जर्वर का उपयोग करके पीएमएसएम ड्राइव से मैकेनिकल पोजीशन सेंसर को हटा दिया जाता है, जो गति और रोटर की स्थिति का अनुमान लगाता है। अनुमानित गति और रोटर की स्थिति का उपयोग तब PMSM ड्राइव के क्षेत्र-उन्मुख नियंत्रण को लागू करने के लिए किया जाता है। स्थिति संवेदक के उन्मूलन से लागत कम हो जाती है और सौर जल पम्पिंग प्रणाली की विश्वसनीयता बढ़ जाती है। यहां तक कि सिस्टम के लोकल-लोड जैसे प्रेशर बूस्टर, कूलिंग फैन, लाइटिंग लोड, फैन-लोड और अन्य को बिजली की आपूर्ति करने का प्रावधान भी सिस्टम में शामिल है। ऐसा भार आवश्यक और अपरिहार्य है क्योंकि यह सौर जल पम्पिंग सिस्टम के सहायक घटकों का प्रतिनिधित्व करता है, जो सिस्टम के सुचारू संचालन के लिए आवश्यक हैं।

MATLAB / Simulink प्लेटफॉर्म पर सिमुलेशन प्रदर्शन करके सौर जल पंपिंग सिस्टम और संबंधित नियंत्रण तकनीकों की प्रस्तुत कॉन्फिगरेशन का प्रदर्शन विश्लेषण किया जाता है। व्यावहारिक ऑपरेटिंग परिदृश्यों के तहत प्रारंभिक, स्थिर-अवस्था और गतिशीलता के दौरान प्रत्येक टोपोलॉजी के लिए कई सिमुलेशन परिणाम प्राप्त और रिपोर्ट किए जाते हैं। इसके अलावा, सभी प्रस्तुत टोपोलॉजी का प्रायोगिक सत्यापन सिस्टम के प्रयोगशाला प्रोटोटाइप पर किया जाता है, और संबंधित परीक्षण के परिणाम रिपोर्ट किए जाते हैं।

TABLE OF CONTENTS

	Page No.
Certificate	i
Acknowledgements	ii
Abstract	v
Table of Contents	vii
List of Figures	xxiii
List of Tables	xlvii
List of Abbreviations	xlviii
List of Symbols	li
CHAPTER I INTRODUCTION	
1.1 General	1
1.2 State of the Art	2
1.3 Objectives and Scope of Work	4
1.3.1 Multilayer Barriers Based Configurations of PMSM for Solar Water Pumping	4
1.3.2 Sensorless PMSM Drive for Standalone Solar Water Pumping System	5
1.3.3 PV Array Fed Grid Interfaced Sensorless PMSM Drive for Water Pumping	5
1.3.4 PV Array and Battery Fed Grid Synchronized Sensorless PMSM Drive for Water Pumping System	5
1.4 Outline of Chapters	5
CHAPTER II LITERATURE REVIEW	
2.1 General	9
2.2 Major Milestones in Development of Solar PV Technology	9
2.3 Standards, Testing and Quality Certification for Solar PV Based Systems	11
2.4 Literature Survey	12
2.4.1 Review of Solar PV Based Water Pumping Systems	12
2.4.1.1 DC Motor Drive Based Solar PV Fed Water Pumping Systems	13
2.4.1.2 Induction Motor Drive Based Solar PV Fed Water Pumping Systems	13
2.4.1.3 SyRM Drive Based Solar PV Fed Water Pumping Systems	14
2.4.1.4 SRM Motor Drive Based Solar PV Fed Water Pumping Systems	14
2.4.1.5 BLDCM Drive Based Solar PV Fed Water Pumping Systems	14
2.4.1.6 PMSM Drive Based Solar PV Fed Water Pumping Systems	15
2.4.2 Review of Techniques for Reduction of PM Demagnetization Risk in PMSM	15
2.4.3 Review of Sensorless Techniques for Solar PV Fed Water Pumping Systems	16
2.4.4 Review of Techniques for Grid Synchronization of Solar Water Pumping Systems	17
2.7 Identified Research Problems	18
2.8 Conclusions	19

CHAPTER III DESIGN AND DEVELOPMENT OF REVERSE SALIENCY PMSM WITH FLUX BARRIERS FOR SOLAR WATER PUMPING SYSTEM

3.1	General	20
3.2	Basic Concept and Configuration of Presented RS-PMSM	20
3.2.1	Basic Concept	20
3.2.2	Configuration of Presented RS-PMSM	21
3.2.3	Reverse Saliency Realization	22
3.3	Design of Presented Reverse Saliency PMSM	23
3.3.1	Calculation of Core Length and Stator Inner Diameter	23
3.3.2	Calculation of PM Volume	24
3.3.3	Selection of Lamination Material	25
3.3.4	Design of Rotor Flux Barriers	26
3.4	FEM Based Performances of Presented RS-PMSM	27
3.4.1	Airgap Flux Density and Back EMF Plot	28
3.4.2	Inductance Characteristics	28
3.4.3	Torque Curves	29
3.4.4	Torque and Output Power Performances	30
3.4.5	Flux Lines	30
3.4.6	PM Demagnetization Analysis	30
3.4.7	Losses and Efficiency Analysis	32
3.4.8	Mechanical Analysis	34
3.5	Test Performances of Presented Reverse Saliency PMSM	35
3.6	Conclusions	39

CHAPTER IV DESIGN OPTIMIZATION OF REVERSE SALIENCY PMSM WITH MULTILAYER BARRIERS FOR SOLAR WATER PUMPING SYSTEM

4.1	General	40
4.2	Basic Concepts and Configurations of Presented Multilayer Barriers Based Reverse Saliency PMSM	41
4.2.1	Presented Reverse Saliency PMSM with Multilayer Barriers	41
4.2.1.1	Topology of Presented RS-PMSM-WMB	41
4.2.1.2	Reverse Saliency Realization in Presented RS-PMSM-WMB	41
4.2.2	Presented Reverse Saliency PMSM with Peripheral Barriers	43
4.2.2.1	Topology of Presented RS-PMSM-WPB	43
4.2.2.2	Improvement in Torque Characteristics of RS-PMSM-WPB	44
4.3	Design Optimization of Presented Multilayer Barriers Based Reverse Saliency PMSM	46
4.3.1	Design Optimization of Presented RS-PMSM-WMB	46
4.3.1.1	Calculation of Core Length and Stator Inner Diameter	46
4.3.1.2	Calculation of PM Volume	47
4.3.1.3	Selection of PM Dimensions	47
4.3.1.4	Selection of Flux Barriers Dimensions	50

4.3.2	Design Optimization of Presented RS-PMSM-WPB	55
4.3.2.1	Calculation of Core Length and Stator Inner Diameter	55
4.3.2.2	Calculation of PM Volume	57
4.3.2.3	Influence of PB and IB on presented RS-PMSM-WPB	57
4.4	FEM Based Performances of Multilayer Barriers Based Reverse Saliency PMSM	64
4.4.1	FEM Based Performances of Presented RS-PMSM-WMB	64
4.4.1.1	Airgap Flux Density and Back EMF Curves	64
4.4.1.2	Inductance Profiles	65
4.4.1.3	Torque Characteristics	66
4.4.1.4	Distribution of Flux Lines	67
4.4.1.5	PM Operating Flux Density	67
4.4.1.6	Assessment of PM Demagnetization Risk	68
4.4.1.7	Torque-Speed and Output Power-Speed Curves	70
4.4.1.8	Output Power and Efficiency Maps	71
4.4.1.9	Mechanical Analysis	71
4.4.2	FEM Based Performances of Presented RS-PMSM-WPB	73
4.4.2.1	Inductance Characteristics	73
4.4.2.2	Torque Characteristics	73
4.4.2.3	PM Operating Flux Density	74
4.4.2.4	Airgap Flux Density and Back EMF Curves	76
4.4.2.5	Loss Analysis	76
4.5	Conclusions	78

CHAPTER V DESIGN AND CONTROL OF SOLAR PV ARRAY FED PMSM DRIVES FOR WATER PUMPING SYSTEM

5.1	General	79
5.2	Configurations of Solar PV Array Fed PMSM Drives for Water Pumping System	79
5.2.1	Configuration of Double-Stage Solar PV Array Fed PMSM Drive with Local Loads for Water Pumping System	79
5.2.2	Configuration of Single-Stage Solar PV Array Fed PMSM Drive with Local Loads for Water Pumping System	81
5.3	Design of Solar PV Array Fed PMSM Drives for Water Pumping System	82
5.3.1	Design of Double-Stage Solar PV Array Fed PMSM Drive with Local Loads for Water Pumping System	82
5.3.1.1	Selection of PMSM	82
5.3.1.2	Design of Water Pump	82
5.3.1.3	Selection of Local Loads	83
5.3.1.4	Design of Solar PV Array	83
5.3.1.5	Design of Boost Converter	84
5.3.1.6	Design of DC Link Capacitor	84
5.3.1.7	Design of Motor-Side VSI	84
5.3.1.8	Design of Load-Side VSC	85

5.3.2	Design of Single-Stage Solar PV Array Fed PMSM Drive with Local Loads for Water Pumping System	85
5.3.2.1	Selection of PMSM and Local-Loads	85
5.3.2.2	Design of Solar PV Array	85
5.3.2.3	Design of DC Link Capacitor	86
5.3.2.4	Design of Motor-Side VSI	87
5.3.2.5	Design of Load-Side VSC	87
5.4	Control of Solar PV Array Fed PMSM Drives for Water Pumping System	87
5.4.1	Control of Double-Stage Solar PV Array Fed PMSM Drive with Local Loads for Water Pumping System	87
5.4.1.1	Boost Converter Based MPPT Control of Solar PV Array	87
5.4.1.2	PMSM Speed and Rotor Position Estimation	89
5.4.1.2.1	Conventional Flux Observers for Estimation of Speed and Rotor Position	90
5.4.1.2.2	AMNF Based Flux Observer for Estimation of Speed and Rotor Position	95
5.4.1.2.3	Comparison of Presented AMNF Based Flux Observer With Conventional Flux Observers	98
5.4.1.3	Control of Motor-Side VSI	100
5.4.1.4	Control of Load-Side VSC	101
5.4.2	Control of Single-Stage Solar PV Array Fed PMSM Drive with Local Loads for Water Pumping System	102
5.4.2.1	MPPT Control of PV Array	102
5.4.2.2	PMSM Speed and Rotor Position Estimation	103
5.4.2.3	Control of Motor-Side VSI	103
5.5	MATLAB/Simulink Based Modeling and Simulation of Solar PV Array Fed PMSM Drives for Water Pumping System	103
5.5.1	MATLAB/Simulink Based Modeling and Simulation of Double-Stage Solar PV Array Fed PMSM Drive with Local Loads for Water Pumping System	103
5.5.2	MATLAB/Simulink Based Modeling and Simulation of Single-Stage Solar PV Array Fed PMSM Drive with Local Loads for Water Pumping System	104
5.6	Hardware Validation of PV Array Fed PMSM Drives for Water Pumping System	104
5.6.1	Development of Signal Conditioning Circuit for Voltage Sensors	106
5.6.2	Development of Signal Conditioning Circuit for Current Sensors	107
5.6.3	Development of Isolation and Amplification Circuit for Gate Drivers	107
5.6.4	Implementation of Control Algorithms by using dSPACE Microlab Box	108
5.7	Results and Discussion	108
5.7.1	Performance of Double-Stage Solar PV Array Fed PMSM Drive with Local Loads for Water Pumping System	108
5.7.1.1	Simulated Performance of Double-Stage Solar PV Array Fed PMSM Drive with Local Loads for Water Pumping System	109
5.7.1.1.1	Starting Performance	109
5.7.1.1.2	Steady-State Performance	110

5.7.1.1.3	Dynamic Performance	111
5.7.1.2	Experimental Performance of Double-Stage Solar PV Array Fed PMSM Drive with Local Loads for Water Pumping System	112
5.7.1.2.1	Starting Performance	112
5.7.1.2.2	Steady-State Performance	113
5.7.1.2.3	Dynamic Performance	114
5.7.1.2.4	MPPT Performance	116
5.7.2	Performance of Single-Stage Solar PV Array Fed PMSM Drive with Local Loads for Water Pumping System	116
5.7.2.1	Simulated Performance of Single-Stage Solar PV Array Fed PMSM Drive with Local Loads for Water Pumping System	116
5.7.2.1.1	Starting Performance	116
5.7.2.1.2	Steady-State Performance	117
5.7.2.1.3	Dynamic Performance	118
5.7.2.2	Experimental Performance of Single-Stage Solar PV Array Fed PMSM Drive with Local Loads for Water Pumping System	120
5.7.2.2.1	Starting Performance	120
5.7.2.2.2	Steady-State Performance	120
5.7.2.2.3	Dynamic Performance	121
5.7.2.2.4	MPPT Performance	122
5.8	Conclusions	123

CHAPTER VI DESIGN AND CONTROL OF SOLAR PV ARRAY AND BATTERY FED PMSM DRIVES FOR WATER PUMPING SYSTEM

6.1	General	124
6.2	Configurations of Solar PV Array and Battery Fed PMSM Drives for Water Pumping System	124
6.2.1	Configuration of Double-Stage Solar PV Array and Battery Fed PMSM Drive with Local Loads for Water Pumping System	125
6.2.2	Configuration of Double-Stage Solar PV Array and Battery with Bidirectional Converter Fed PMSM Drive with Local Loads for Water Pumping System	125
6.2.3	Configuration of Single-Stage Solar PV Array and Battery with Bidirectional Converter Fed PMSM Drive with Local Loads for Water Pumping System	126
6.3	Design of Solar PV Array and Battery Fed PMSM Drives for Water Pumping System	126
6.3.1	Design of Double-Stage Solar PV Array and Battery Fed PMSM Drive with Local Loads for Water Pumping System	127
6.3.1.1	Selection of PMSM and Local-Loads	127
6.3.1.2	Design of Water Pump	127
6.3.1.3	Design of Solar PV Array	127
6.3.1.4	Design of Boost Converter	128
6.3.1.5	Design of DC Link Capacitor	128
6.3.1.6	Design of BES	129

6.3.1.7	Design of Motor-Side VSI	130
6.3.1.8	Design of Load-Side VSC	130
6.3.2	Design of Double-Stage Solar PV Array and Battery with Bidirectional Converter Fed PMSM Drive with Local Loads for Water Pumping System	130
6.3.2.1	Design of BES	131
6.3.2.2	Design of Bidirectional DC-DC Converter	132
6.3.3	Design of Single-Stage Solar PV Array and Battery with Bidirectional Converter Fed PMSM Drive with Local Loads for Water Pumping System	132
6.3.3.1	Design of Solar PV Array	133
6.4	Control of Solar PV Array and Battery Fed PMSM Drives for Water Pumping System	134
6.4.1	Control of Double-Stage Solar PV Array and Battery Fed PMSM Drive with Local Loads for Water Pumping System	134
6.4.1.1	Boost Converter Based MPPT Control of PV Array	134
6.4.1.2	PMSM Speed and Rotor Angle Estimation	134
6.4.1.3	Control of Motor Side VSI	134
6.4.1.4	Control of Load-Side VSC	134
6.4.2	Control of Double-Stage Solar PV Array and Battery with Bidirectional Converter Fed PMSM Drive with Local Loads for Water Pumping System	134
6.4.2.1	Control of Bidirectional Converter	135
6.4.3	Control of Single-Stage Solar PV Array and Battery with Bidirectional Converter Fed PMSM Drive with Local Loads for Water Pumping System	135
6.4.3.1	MPPT Control of PV Array	136
6.4.3.2	Control of Bidirectional Converter	136
6.5	MATLAB/Simulink Based Modeling and Simulation of Solar PV Array and Battery Fed PMSM Drives for Water Pumping System	136
6.6	Hardware Validation of Solar PV Array and Battery Fed PMSM Drives for Water Pumping System	138
6.7	Results and Discussion	139
6.7.1	Performance of Double-Stage Solar PV Array and Battery Fed PMSM Drive with Local Loads for Water Pumping System	139
6.7.1.1	Simulated Performance	139
6.7.1.2	Experimental Performance	144
6.7.2	Performance of Double-Stage Solar PV Array and Battery with Bidirectional Converter Fed PMSM Drive with Local Loads for Water Pumping System	148
6.7.2.1	Simulated Performance	149
6.7.2.2	Experimental Performance	153
6.7.3	Performance of Single-Stage Solar PV Array and Battery with Bidirectional Converter Fed PMSM Drive with Local Loads for Water Pumping System	158
6.7.3.1	Simulated Performance	158
6.7.3.2	Experimental Performance	162
6.8	Conclusions	168

CHAPTER VII DESIGN AND CONTROL OF SINGLE-PHASE GRID-INTERFACED SOLAR PV ARRAY FED PMSM DRIVES FOR WATER PUMPING SYSTEM

7.1	General	169
7.2	Configurations of Single-Phase Grid-Interfaced Solar PV Array Fed PMSM Drives for Water Pumping System	170
7.2.1	Configuration of Single-Phase Grid-Interfaced Double-Stage Solar PV Array Fed PMSM Drive with Local Loads for Water Pumping System	170
7.2.2	Configuration of Single-Phase Grid-Synchronized Single-Stage Solar PV Array Fed PMSM Drive with Local Loads for Water Pumping System	171
7.3	Design of Single-Phase Grid-Interfaced Solar PV Array Fed PMSM Drives for Water Pumping System	172
7.3.1	Design of Single-Phase Grid-Interfaced Double-Stage Solar PV Array Fed PMSM Drive with Local Loads for Water Pumping System	172
7.3.1.1	Selection of PMSM and Local-Loads	172
7.3.1.2	Selection of Water Pump	172
7.3.1.3	Design of Solar PV Array	172
7.3.1.4	Design of Boost Converter	173
7.3.1.5	Design of DC Link Capacitor	173
7.3.1.6	Design of Motor-Side VSI	173
7.3.1.7	Design of Grid-Side VSC	173
7.3.1.8	Design of Interfacing Inductor	173
7.3.1.9	Design of RC Filter	174
7.3.2	Design of Single-Phase Grid-Synchronized Single-Stage Solar PV Array Fed PMSM Drive with Local Loads for Water Pumping System	174
7.3.2.1	Design of Solar PV Array	174
7.3.2.2	Design of Synchronization Unit	174
7.4	Control of Single-Phase Grid-Interfaced Solar PV Array Fed PMSM Drives for Water Pumping System	175
7.4.1	Control of Single-Phase Grid-Interfaced Double-Stage Solar PV Array Fed PMSM Drive with Local Loads for Water Pumping System	175
7.4.1.1	Control of Grid-Side VSC	175
7.4.1.1.1	Analysis of AMNF-FLL Structure	177
7.4.1.2	Control of Motor-Side VSI	180
7.4.2	Control of Single-Phase Grid-Synchronized Single-Stage Solar PV Array Fed PMSM Drive with Local Loads for Water Pumping System	180
7.4.2.1	Speed Control of PMSM	181
7.4.2.2	Control of Motor-Side VSI	181
7.4.2.3	Control of Grid-Side VSC	181
7.4.2.4	Control of Synchronization Unit	182
7.5	MATLAB/Simulink Based Modeling and Simulation of Single-Phase Grid-Interfaced Solar PV Array Fed PMSM Drives for Water Pumping System	183

7.6	Hardware Validation of Single-Phase Grid-Interfaced Solar PV Array Fed PMSM Drives for Water Pumping System	184
7.7	Results and Discussion	185
7.7.1	Performance of Single-Phase Grid-Interfaced Double-Stage Solar PV Array Fed PMSM Drive with Local Loads for Water Pumping System	185
7.7.1.1	Simulated Performance	185
7.7.1.2	Experimental Performance	192
7.7.2	Performance of Single-Phase Grid-Synchronized Single-Stage Solar PV Array Fed PMSM Drive with Local Loads for Water Pumping System	201
7.7.2.1	Simulated Performance	202
7.7.2.2	Experimental Performance	209
7.8	Conclusions	215

CHAPTER VIII DESIGN AND CONTROL OF SINGLE-PHASE GRID-INTERFACED SOLAR PV ARRAY AND BATTERY FED PMSM DRIVES FOR WATER PUMPING SYSTEM

8.1	General	217
8.2	Configurations of Single-Phase Grid-Interfaced Solar PV Array and Battery Fed PMSM Drives for Water Pumping System	218
8.2.1	Configuration of Single-Phase Grid-Interfaced Double-Stage Solar PV Array and Battery Fed PMSM Drive for Water Pumping System	218
8.2.2	Configuration of Single-Phase Grid-Interfaced Double-Stage Solar PV Array and Battery with BDC Fed PMSM Drive for Water Pumping System	218
8.2.3	Configuration of Single-Phase Grid-Interfaced Single-Stage Solar PV Array and Battery with BDC Fed PMSM Drive for Water Pumping System	219
8.2.4	Configuration of Single-Phase Grid-Interfaced Double-Stage PV Array and Battery Fed PMSM Drive with Local Loads for Water Pumping System	220
8.2.5	Configuration of Single-Phase Grid-Interfaced Double-Stage PV Array and Battery with Bidirectional Converter Fed PMSM Drive with Local Loads for Water Pumping System	221
8.2.6	Configuration of Single-Phase Grid-Synchronized Single-Stage Solar PV Array and Battery with Bidirectional Converter Fed PMSM Drive with Local Loads for Water Pumping System	221
8.3	Design of Single-Phase Grid-Interfaced Solar PV Array and Battery Fed PMSM Drives for Water Pumping System	222
8.3.1	Design of Single-Phase Grid-Interfaced Double-Stage Solar PV Array and Battery Fed PMSM Drive for Water Pumping System	222
8.3.1.1	Selection of PMSM	222
8.3.1.2	Design of Water Pump	222
8.3.1.3	Design of Solar PV Array	222
8.3.1.4	Design of Boost Converter	223
8.3.1.5	Design of DC Link Capacitor	223
8.3.1.6	Design of BES	223

	8.3.1.7	Design of Motor-Side VSI	223	
	8.3.1.8	Design of Grid-Side VSC	223	
	8.3.1.9	Design of Interfacing Inductor	223	
	8.3.1.10	Design of RC Filter	223	
8.3.2		Design of Single-Phase Grid-Interfaced Double-Stage Solar PV Array and Battery with BDC Fed PMSM Drive for Water Pumping System	223	
	8.3.2.1	Design of BES	223	
	8.3.2.2	Design of Bidirectional Converter	224	
8.3.3		Design of Single-Phase Grid-Interfaced Single-Stage Solar PV Array and Battery with BDC Fed PMSM Drive for Water Pumping System	224	
	8.3.3.1	Design of Solar PV Array	224	
8.3.4		Design of Single-Phase Grid-Interfaced Double-Stage Solar PV Array and Battery Fed PMSM Drive with Local Loads for Water Pumping System	224	
	8.3.4.1	Selection of Local Loads	225	
	8.3.4.2	Design of PV array	225	
	8.3.4.3	Design of BES	225	
	8.3.4.4	Design of DC Link Capacitor	225	
	8.3.4.5	Design of Grid Side VSC	225	
8.3.5		Design of Single-Phase Grid-Interfaced Double-Stage Solar PV Array and Battery with Bidirectional Converter Fed PMSM Drive with Local Loads for Water Pumping System	225	
	8.3.5.1	Design of BES	225	
	8.3.5.2	Design of Bidirectional Converter	226	
8.3.6		Design of Single-Phase Grid-Synchronized Single-Stage Solar PV Array and Battery with Bidirectional Converter Fed PMSM Drive with Local Loads for Water Pumping System	226	
	8.3.6.1	Design of Solar PV Array	226	
	8.3.6.2	Design of Synchronization Unit	226	
8.4		Control of Single-Phase Grid-Interfaced Solar PV Array and Battery Fed PMSM Drives for Water Pumping System	226	
	8.4.1	Control of Single-Phase Grid-Interfaced Double-Stage Solar PV Array and Battery Fed PMSM Drive for Water Pumping System	226	
		8.4.1.1	Control of Grid-Side VSC	227
		8.4.1.2	Speed Control of PMSM	227
		8.4.1.3	Control of Grid-Side VSC	227
8.4.2		Control of Single-Phase Grid-Interfaced Double-Stage Solar PV Array and Battery with BDC Fed PMSM Drive for Water Pumping System	227	
	8.4.2.1	Control of Bidirectional Converter	228	
8.4.3		Control of Single-Phase Grid-Interfaced Single-Stage Solar PV Array and Battery with BDC Fed PMSM Drive for Water Pumping System	228	
	8.4.3.1	MPPT Control of PV Array	228	
	8.4.3.2	Control of Bidirectional Converter	228	

8.4.4	Control of Single-Phase Grid-Interfaced Double-Stage Solar PV Array and Battery Fed PMSM Drive with Local Loads for Water Pumping System	228
8.4.4.1	Control of Grid-Side VSC	229
8.4.5	Control of Single-Phase Grid-Interfaced Double-Stage Solar PV Array and Battery with Bidirectional Converter Fed PMSM Drive with Local Loads for Water Pumping System	229
8.4.5.1	Control of Bidirectional Converter	229
8.4.6	Control of Single-Phase Grid-Synchronized Single-Stage Solar PV Array and Battery with Bidirectional Converter Fed PMSM Drive with Local Loads for Water Pumping System	229
8.4.6.1	Control of Grid-Side VSC	230
8.4.6.2	Control of Synchronizing Unit	230
8.5	MATLAB/Simulink Based Modeling and Simulation of Single-Phase Grid-Interfaced PV Array and Battery Fed PMSM Drives for Water Pumping System	230
8.6	Hardware Validation of Single-Phase Grid-Interfaced Solar PV Array and Battery Fed PMSM Drives for Water Pumping System	233
8.7	Results and Discussion	
8.7.1	Performance of Single-Phase Grid-Interfaced Double-Stage Solar PV Array and Battery Fed PMSM Drive for Water Pumping System	233
8.7.1.1	Simulated Performance of Single Phase Grid Interfaced Double Stage Solar PV Array and Battery Fed PMSM Drive for Water Pumping System	234
8.7.1.1.1	Simulated Performance When Grid is Available	234
8.7.1.1.2	Simulated Performance When Grid is Not Available	236
8.7.1.2	Experimental Performance of Single Phase Grid Interfaced Double Stage Solar PV Array and Battery Fed PMSM Drive for Water Pumping System	238
8.7.1.2.1	Experimental Performance When Grid is Available	238
8.7.1.2.2	Experimental Performance When Grid is Not Available	244
8.7.2	Performance of Single-Phase Grid-Interfaced Double-Stage Solar PV Array and Battery with BDC Fed PMSM Drive for Water Pumping System	246
8.7.2.1	Simulated Performance of Single-Phase Grid-Interfaced Double-Stage Solar PV Array and Battery with BDC Fed PMSM Drive for Water Pumping System	246
8.7.2.1.1	Simulated Performance When Grid is Available	246
8.7.2.1.2	Simulated Performance When Grid is Not Available	249
8.7.2.2	Experimental Performance of Single-Phase Grid-Interfaced Double-Stage Solar PV Array and Battery with BDC Fed PMSM Drive for Water Pumping System	251
8.7.2.2.1	Experimental Performance When Grid is Available	251
8.7.2.2.2	Experimental Performance When Grid is Not Available	257

8.7.3	Performance of Single-Phase Grid-Interfaced Single-Stage Solar PV Array and Battery with BDC Fed PMSM Drive for Water Pumping System	259
8.7.3.1	Simulated Performance of Single-Phase Grid-Interfaced Single-Stage Solar PV Array and Battery with BDC Fed PMSM Drive for Water Pumping System	259
8.7.3.1.1	Simulated Performance When Grid is Available	259
8.7.3.1.2	Simulated Performance When Grid is Not Available	262
8.7.3.2	Experimental Performance of Single-Phase Grid-Interfaced Single-Stage Solar PV Array and Battery with BDC Fed PMSM Drive for Water Pumping System	264
8.7.3.2.1	Experimental Performance When Grid is Available	264
8.7.3.2.2	Experimental Performance When Grid is Not Available	270
8.7.4	Performance of Single-Phase Grid-Interfaced Double-Stage PV Array and Battery Fed PMSM Drive with Local Loads for Water Pumping System	272
8.7.4.1	Simulated Performance of Single-Phase Grid-Interfaced Double-Stage PV Array and Battery Fed PMSM Drive with Local Loads for Water Pumping System	272
8.7.4.1.1	Simulated Performance When Grid is Available	272
8.7.4.1.2	Simulated Performance When Grid is Not Available	275
8.7.4.2	Experimental Performance of Single-Phase Grid-Interfaced Double-Stage PV Array and Battery Fed PMSM Drive with Local Loads for Water Pumping System	276
8.7.4.2.1	Experimental Performance When Grid is Available	277
8.7.4.2.2	Experimental Performance When Grid is Not Available	282
8.7.5	Performance of Single-Phase Grid-Interfaced Double-Stage Solar PV Array and Battery with Bidirectional Converter Fed PMSM Drive with Local Loads for Water Pumping System	284
8.7.5.1	Simulated Performance of Single-Phase Grid-Interfaced Double-Stage Solar PV Array and Battery with Bidirectional Converter Fed PMSM Drive with Local Loads for Water Pumping System	285
8.7.5.1.1	Simulated Performance When Grid is Available	285
8.7.5.1.2	Simulated Performance When Grid is Not Available	288
8.7.5.2	Experimental Performance of Single-Phase Grid-Interfaced Double-Stage Solar PV Array and Battery with Bidirectional Converter Fed PMSM Drive with Local Loads for Water Pumping System	289
8.7.5.2.1	Experimental Performance When Grid is Available	290
8.7.5.2.2	Experimental Performance When Grid is Not Available	295

8.7.6	Performance of Single-Phase Grid-Synchronized Single-Stage Solar PV Array and Battery with Bidirectional Converter Fed PMSM Drive with Local Loads for Water Pumping System	296
8.7.6.1	Simulated Performance of Single-Phase Grid-Synchronized Single-Stage Solar PV Array and Battery with Bidirectional Converter Fed PMSM Drive with Local Loads for Water Pumping System	296
8.7.6.1.1	Simulated Performance of System Under GCM	297
8.7.6.1.2	Simulated Performance of System Under IDM	298
8.7.6.1.3	Simulated Performance Under Seamless Mode Transition	300
8.7.6.2	Experimental Performance of Single-Phase Grid-Synchronized Single-Stage Solar PV Array and Battery with Bidirectional Converter Fed PMSM Drive with Local Loads for Water Pumping System	301
8.7.6.2.1	MPPT Performances	301
8.7.6.2.2	Experimental Performance of System Under GCM	302
8.7.6.2.3	Experimental Performance of System Under IDM	303
8.7.6.2.4	Experimental Performance Under Seamless Mode Transition	305
8.8	Conclusions	306

CHAPTER IX DESIGN AND CONTROL OF THREE-PHASE GRID-INTERFACED SOLAR PV ARRAY FED PMSM DRIVES FOR WATER PUMPING SYSTEM

9.1	General	307
9.2	Configurations of Three-Phase Grid-Interfaced Solar PV Array Fed PMSM Drives for Water Pumping System	308
9.2.1	Configuration of Three-Phase Grid-Interfaced Double-Stage Solar PV Array Fed PMSM Drive with Local Loads for Water Pumping System	308
9.2.2	Configuration of Three-Phase Grid-Synchronized Single-Stage Solar PV Array Fed PMSM Drive with Local Loads for Water Pumping System	309
9.3	Design of Three-Phase Grid-Interfaced Solar PV Array Fed PMSM Drives for Water Pumping System	309
9.3.1	Design of Three-Phase Grid-Interfaced Double-Stage Solar PV Array Fed PMSM Drive with Local Loads for Water Pumping System	309
9.3.1.1	Selection of PMSM and Local-Loads	310
9.3.1.2	Design of Water Pump	310
9.3.1.3	Design of Solar PV Array	310
9.3.1.4	Design of Boost Converter	310
9.3.1.5	Design of Motor-Side VSI	310
9.3.1.6	Design of DC Link Capacitor	310
9.3.1.7	Design of Grid-Side VSC	310

9.3.1.8	Design of Interfacing Inductor	311
9.3.1.9	Design of RC Filter	311
9.3.2	Design of Three-Phase Grid-Synchronized Single-Stage Solar PV Array Fed PMSM Drive with Local Loads for Water Pumping System	311
9.3.2.1	Design of Solar PV Array	311
9.3.2.2	Design of Synchronization Unit	312
9.4	Control of Three-Phase Grid-Interfaced Solar PV Array Fed PMSM Drives for Water Pumping System	312
9.4.1	Control of Three-Phase Grid-Interfaced Double-Stage Solar PV Array Fed PMSM Drive with Local Loads for Water Pumping System	312
9.4.1.1	Control of Grid-Side VSC	313
9.4.1.2	Speed Control of PMSM	314
9.4.1.3	Control of Motor-Side VSI	314
9.4.2	Control of Three-Phase Grid-Synchronized Single-Stage Solar PV Array Fed PMSM Drive with Local Loads for Water Pumping System	315
9.4.2.1	Control of Grid-Side VSC	315
9.4.2.2	Control of Synchronizing Unit	316
9.5	MATLAB/Simulink Based Modeling and Simulation of Three-Phase Grid-Interfaced Solar PV Array Fed PMSM Drives for Water Pumping System	318
9.6	Hardware Validation of Three-Phase Grid-Interfaced Solar PV Array Fed PMSM Drives for Water Pumping System	319
9.7	Results and Discussion	319
9.7.1	Performance of Three-Phase Grid-Interfaced Double-Stage Solar PV Array Fed PMSM Drive with Local Loads for Water Pumping System	319
9.7.1.1	Simulated Performance	320
9.7.1.2	Experimental Performance	326
9.7.2	Performance of Three-Phase Grid-Synchronized Single-Stage Solar PV Array Fed PMSM Drive with Local Loads for Water Pumping System	336
9.7.2.1	Simulated Performance	336
9.7.2.2	Experimental Performance	343
9.8	Conclusions	351

CHAPTER X DESIGN AND CONTROL OF THREE-PHASE GRID-INTERFACED SOLAR PV ARRAY AND BATTERY FED PMSM DRIVES FOR WATER PUMPING SYSTEM

10.1	General	353
10.2	Configurations of Three-Phase Grid-Interfaced Solar PV Array and Battery Fed PMSM Drives for Water Pumping System	354
10.2.1	Configuration of Three-Phase Grid-Interfaced Double-Stage Solar PV Array and Battery Fed PMSM Drive for Water Pumping System	354
10.2.2	Configuration of Three-Phase Grid-Interfaced Double-Stage Solar PV Array and Battery with Bidirectional Converter Fed PMSM Drive for Water Pumping System	354

10.2.3	Configuration of Three-Phase Grid-Interfaced Single-Stage Solar PV Array and Battery with Bidirectional Converter Fed PMSM Drive for Water Pumping System	355
10.2.4	Configuration of Three-Phase Grid-Interfaced Double-Stage PV Array and Battery Fed PMSM Drive with Local Loads for Water Pumping System	356
10.2.5	Configuration of Three-Phase Grid-Interfaced Double-Stage Solar PV Array and Battery with Bidirectional Converter Fed PMSM Drive with Local Loads for Water Pumping System	357
10.2.6	Configuration of Three-Phase Grid-Synchronized Single-Stage Solar PV Array and Battery with Bidirectional Converter Fed PMSM Drive with Local Loads for Water Pumping System	357
10.3	Design of Three-Phase Grid-Interfaced Solar PV Array and Battery Fed PMSM Drives for Water Pumping System	358
10.3.1	Design of Three-Phase Grid-Interfaced Double-Stage Solar PV Array and Battery Fed PMSM Drive for Water Pumping System	358
10.3.1.1	Selection of PMSM	358
10.3.1.2	Design of Water Pump	359
10.3.1.3	Design of Solar PV Array	359
10.3.1.4	Design of Boost Converter	359
10.3.1.5	Design of DC Link Capacitor	359
10.3.1.6	Design of BES	359
10.3.1.7	Design of Motor-Side VSI	359
10.3.1.8	Design of Grid-Side VSC	359
10.3.1.9	Design of Interfacing Inductor	359
10.3.1.10	Design of RC Filter	359
10.3.2	Design of Three-Phase Grid-Interfaced Double-Stage Solar PV Array and Battery with BDC Fed PMSM Drive for Water Pumping System	360
10.3.2.1	Design of BES	360
10.3.2.2	Design of Bidirectional Converter	360
10.3.3	Design of Three-Phase Grid-Interfaced Single-Stage Solar PV Array and Battery with BDC Fed PMSM Drive for Water Pumping System	360
10.3.3.1	Design of Solar PV Array	360
10.3.4	Design of Three-Phase Grid-Interfaced Double-Stage Solar PV Array and Battery Fed PMSM Drive with Local Loads for Water Pumping System	361
10.3.4.1	Selection of Local Loads	361
10.3.4.2	Design of PV Array	361
10.3.4.3	Design of BES	361
10.3.4.4	Design of DC Link Capacitor	361
10.3.4.5	Design of Grid-Side VSC	361
10.3.5	Design of Three-Phase Grid-Interfaced Double-Stage Solar PV Array and Battery with Bidirectional Converter Fed PMSM Drive with Local Loads for Water Pumping System	362
10.3.5.1	Design of BES	362

10.3.5.2	Design of Bidirectional Converter	362
10.3.6	Design of Three-Phase Grid-Synchronized Single-Stage Solar PV Array and Battery with Bidirectional Converter Fed PMSM Drive with Local Loads for Water Pumping System	362
10.3.6.1	Design of Solar PV Array	362
10.3.6.2	Design of Synchronization Unit	363
10.4	Control of Three-Phase Grid-Interfaced Solar PV Array and Battery Fed PMSM Drives for Water Pumping System	363
10.4.1	Control of Three-Phase Grid-Interfaced Double-Stage Solar PV Array and Battery Fed PMSM Drive for Water Pumping System	363
10.4.1.1	Control of Grid-Side VSC	363
10.4.1.2	Speed Control of PMSM	363
10.4.1.3	Control of Motor-Side VSI	363
10.4.2	Control of Three-Phase Grid-Interfaced Double-Stage Solar PV Array and Battery with BDC Fed PMSM Drive for Water Pumping System	364
10.4.2.1	Control of Bidirectional Converter	364
10.4.3	Control of Three-Phase Grid-Interfaced Single-Stage Solar PV Array and Battery with BDC Fed PMSM Drive for Water Pumping System	364
10.4.3.1	MPPT Control of PV Array	364
10.4.3.2	Control of Bidirectional Converter	365
10.4.4	Control of Three-Phase Grid-Interfaced Double-Stage Solar PV Array and Battery Fed PMSM Drive with Local Loads for Water Pumping System	365
10.4.4.1	Control of Grid-Side VSC	365
10.4.5	Control of Three-Phase Grid-Interfaced Double-Stage Solar PV Array and Battery with Bidirectional Converter Fed PMSM Drive with Local Loads for Water Pumping System	365
10.4.5.1	Control of Bidirectional Converter	366
10.4.6	Control of Three-Phase Grid-Interfaced Single-Stage Solar PV Array and Battery with Bidirectional Converter Fed PMSM Drive with Local Loads for Water Pumping System	366
10.4.6.1	Control of Grid-Side VSC	366
10.4.6.2	Control of Synchronizing Unit	366
10.5	MATLAB/Simulink Based Modeling and Simulation of Three-Phase Grid-Interfaced PV Array and Battery Fed PMSM Drives for Water Pumping System	367
10.6	Hardware Validation of Three-Phase Grid-Interfaced Solar PV Array and Battery Fed PMSM Drives for Water Pumping System	369
10.7	Results and Discussion	369
10.7.1	Performance of Three-Phase Grid-Interfaced Double-Stage Solar PV Array and Battery Fed PMSM Drive for Water Pumping System	370
10.7.1.1	Simulated Performance	370
10.7.1.2	Experimental Performance	374
10.7.2	Performance of Three-Phase Grid-Interfaced Double-Stage Solar PV Array and Battery with BDC Fed PMSM Drive for Water Pumping System	381

10.7.2.1	Simulated Performance	381
10.7.2.2	Experimental Performance	386
10.7.3	Performance of Three-Phase Grid-Interfaced Single-Stage Solar PV Array and Battery with BDC Fed PMSM Drive for Water Pumping System	393
10.7.3.1	Simulated Performance	393
10.7.3.2	Experimental Performance	398
10.7.4	Performance of Three-Phase Grid-Interfaced Double-Stage Solar PV Array and Battery Fed PMSM Drive with Local Loads for Water Pumping System	404
10.7.4.1	Simulated Performance	405
10.7.4.2	Experimental Performance	409
10.7.5	Performance of Three-Phase Grid-Interfaced Double-Stage Solar PV Array and Battery with Bidirectional Converter Fed PMSM Drive with Local Loads for Water Pumping System	416
10.7.5.1	Simulated Performance	416
10.7.5.2	Experimental Performance	421
10.7.6	Performance of Three-Phase Grid-Synchronized Single-Stage Solar PV Array and Battery with Bidirectional Converter Fed PMSM Drive with Local Loads for Water Pumping System	426
10.7.6.1	Simulated Performance	426
10.7.6.2	Experimental Performance	431
10.8	Conclusions	436

CHAPTER XI MAIN CONCLUSIONS AND SUGGESTIONS FOR FURTHER WORK

11.1	General	437
11.2	Main Conclusions and Contributions	438
11.3	Suggestions for Further Work	440

REFERENCES	442
-------------------	-----

APPENDICES	462
-------------------	-----

LIST OF PUBLICATIONS	466
-----------------------------	-----

AUTHOR BIO-DATA	469
------------------------	-----

LIST OF FIGURES

- Fig. 3.1 Illustration of (a) phasor diagram and (b) current-voltage constraint curve
- Fig. 3.2 Cross-sectional view of (a) RS-PMSM, and (b) CS-PMSM
- Fig. 3.3 Flux-path and equivalent magnetic circuit of (a) d-axis, and (b) q-axis
- Fig. 3.4 Specifications of standard steel grades. (a) Core loss, and (b) thickness
- Fig. 3.5 Evolution of RS-PMSM rotor. (a) primary design, (b) intervening design, (c) final design
- Fig. 3.6 Flowchart illustrating RS-PMSM design process
- Fig. 3.7 Performance indices. (a) Airgap flux density, B_{ag} and (b) back EMF, e_a
- Fig. 3.8 Inductances variation with (a) current angle, δ and (b) peak current, I_m
- Fig. 3.9 Average torque, T_{av} variation vs (a) current angle, δ , and (b) peak current, I_m
- Fig. 3.10 Torque ripple variation vs (a) current angle, δ and (b) peak current, I_m
- Fig. 3.11 (a) Torque versus speed, and (b) output-power versus speed curves
- Fig. 3.12 Flux lines at no-load in (a) RS-PMSM, and (b) CS-PMSM
- Fig. 3.13 Illustration of PM operating points in RS-PMSM and CS-PMSM
- Fig. 3.14 PM flux density distribution at (a-b) $I_m = 10$ A, (c-d) $I_m = 20$ A, and (e-f) $I_m = 30$ A in RS-PMSM (a,c,e) and CS-PMSM (b,d,f)
- Fig. 3.15 Flux density at center point P of PM, B_{PM} for (a) RS-PMSM, and (b) CS-PMSM at different I_m
- Fig. 3.16 Variation of losses in RS-PMSM with I_m and δ . (a) PM eddy current loss, (b) rotor eddy current loss, (c) stator eddy current loss, (d) rotor hysteresis loss, and (e) stator hysteresis loss (f) copper loss, and (g) sum all losses
- Fig. 3.17 Illustration of RS PMSM, (a) total losses, (b) output power, and (c) efficiency
- Fig. 3.18 Mechanical performances of RS-PMSM. (a)-(b) Deformation, and (c)-(d) Von-Mises stress at (a),(c) 1500 rpm, and (b),(d) 3000 rpm
- Fig. 3.19 Illustration of (a) rotor stamping, (b) rotor stack, (c) stator stack, (d) rotor assembly, and (e) RS-PMSM prototype
- Fig. 3.20 RS-PMSM Back EMF curves at (a) 314 rad/s, and (b) 200 rad/s
- Fig. 3.21 FEA and experimental (a) stator current, (b) power factor angle, (c) power factor, (d) input power, (e) torque, and (f) efficiency of the RS-PMSM
- Fig. 3.22 RS-PMSM electrical parameters at stator current equal to (a) 1.84 A, (b) 4.03 A (c) 5.28 A (d) 7.15 A (e) 7.85 A, and (f) 9.39 A
- Fig. 4.1 Configuration of (a) RS-PMSM-WMB, and (b) CS-PMSM

- Fig. 4.2 Representation of (a) dq -axes flux path, and (b) dq -axes simplified magnetic circuits
- Fig. 4.3 Configuration. (a) existing PMSM, and (b) presented RS-PMSM-WPB
- Fig. 4.4 dq -axes magnetic circuits. (a) existing PMSM and, (b) RS-PMSM-WPB
- Fig. 4.5 Rotor of RS-PMSM-WPB (a) with PB, and (b) without PB
- Fig. 4.6 RS-PMSM-WPB magnetic circuits. (a) with PB, and (b) without PB
- Fig.4.7 RS-PMSM-WPB. (a) torque enhancement, and (b) phasor diagram
- Fig. 4.8 Main dimensions of RS-PMSM-WMB
- Fig. 4.9 Variation of (a) average torque, T_{av} , (b) core-losses, P_{cl} , (c) PM volume, V_{PM} with l_m and t_m , and (d) T_{av} with V_{PM} and P_{cl}
- Fig. 4.10 Selection of PM dimensions on the basis of (a) average torque, T_{av} , (b) coreloss, P_{cl} , and (c) volume of PM, V_{PM} . Variation of (d) saliency difference, δL with l_m and t_m
- Fig. 4.11 Variation of (a) saliency difference, δL , (b) torque ripple, δT , and (c) average torque, T_{av} with r_i and d at different value
- Fig. 4.12 Variation of (a) saliency difference, δL , (b) torque ripple, δT , and (c) average torque, T_{av} with r_i and d at $b_r = 2.5$ mm
- Fig. 4.13 Values of (a) GCC, (b) GCG, (c) performance indices, and (d) design variables for top five design sets
- Fig. 4.14 Flowchart of design and optimization process for RS-PMSM-WMB
- Fig. 4.15 RS-PMSM-WPB rotor. (a) PB thickness, $t_{PB} = 0$ mm, and (b) $t_{PB} = 4$ mm
- Fig. 4.16 Influence of PB thickness, t_{PB} on (a) inductances, (b) torque and torque ripple, (c) instantaneous and, (d) average PM flux density
- Fig. 4.17 RS-PMSM-WPB rotor. (a) PB angle, $\alpha_{pb} = -4^\circ$ mech., and (b) $\alpha_{pb} = 4^\circ$ mech.
- Fig. 4.18 Influence of PB angle, α_{PB} on (a) inductances, (b) torque and torque ripple, (c) instantaneous and, (d) average PM flux density
- Fig. 4.19 RS-PMSM-WPB rotor. (a) IB thickness, $t_{IB} = 1$ mm, and (b) $t_{IB} = 5$ mm
- Fig. 4.20 Influence of IB thickness, t_{IB} on (a) inductances, (b) torque and torque ripple, (c) instantaneous and, (d) average PM flux density
- Fig. 4.21 RS-PMSM-WPB rotor (a) IB inner radius, $r_i = 0$ mm, and (b) $r_i = 1$ mm
- Fig. 4.22 Influence of IB inner radius, r_i on (a) inductance, (b) torque and torque ripple, (c) instantaneous, and (d) average PM flux density
- Fig. 4.23 RS-PMSM-WPB rotor with (a) IB rib, $h_{IB} = 1$ mm, and (b) $h_{IB} = 8$ mm
- Fig. 4.24 Influence of IB rib, h_{IB} on (a) inductances, (b) torque and torque ripple, (c) instantaneous PM flux density, and (d) average PM flux density
- Fig. 4.25 No-load performances. (a) Airgap flux density, B_{ag} , (b) phase a back EMF, and (c) its harmonic spectrum for RS-PMSM-WMB and CS-PMSM

- Fig. 4.26 Direct and quadrature axes inductance variation with (a) peak current, I_m , and (b) current angle, δ for RS-PMSM-WMB and CS-PMSM
- Fig. 4.27 Torque profiles. (a) T_{av} vs δ , and (b) δT vs δ for RS-PMSM-WMB and CS-PMSM where T_{av} is average torque, δT is torque ripple, and δ is current angle
- Fig. 4.28 Variation of (a) saliency difference, δL , and (b) torque ripples, δT with current angle, δ and peak current, I_m for RS-PMSM-WMB and CS-PMSM
- Fig. 4.29 A Flux line distribution at no-load. (a) RS-PMSM-WMB, and (b) CS-PMSM
- Fig. 4.30 Magnetic flux density distribution in rotor of (a) RS-PMSM-WMB, and (b) CS-PMSM at rated load
- Fig. 4.31 (a) PM operating points, and (b) maximum torque, T_{max} versus peak current, I_m curves of RS-PMSM-WMB and CS-PMSM
- Fig. 4.32 PM flux density plot at (a-b) $I_m = 14A$, (c-d) $I_m = 21A$, (e-f) $I_m = 28A$, and (g-h) $I_m = 35A$ of RS-PMSM-WMB (a,c,e,g) and CS-PMSM (b,d,f,h)
- Fig. 4.33 PM flux density, B_{pm} at point Q in (a) RS-PMSM-WMB, and (b) CS-PMSM under different peak currents
- Fig. 4.34 (a) Torque vs speed, and (b) output power vs speed curves for both the RS-PMSM-WMB and CS-PMSM
- Fig. 4.35 RS-PMSM-WMB. (a) Output Power, P_o and (b) Efficiency, η maps
- Fig. 4.36 Mechanical analysis of presented RS-PMSM-WMB. (a)-(b) Von-Mises stress, and (c)-(d) Deformation at (a),(c) 3000 rpm, and (b),(d) 4500 rpm
- Fig. 4.37 RS-PMSM-WPB inductances with and without PB. Variation with (a) δ , and (b) I_m
- Fig. 4.38 RS-PMSM-WPB average and reluctance torques with and without PB. Variation with (a) δ , and (b) I_m
- Fig. 4.39 RS-PMSM-WPB torque ripple with and without PB. Variation with (a) δ , and (b) I_m
- Fig. 4.40 Distribution of flux density in (a) conventional PMSM, and (b) presented RS-PMSM-WPB at various peak current values
- Fig. 4.41 Flux density at center of PM in RS-PMSM-WPB and conventional PMSM for different peak currents. (a) 10 A, (b) 15 A, (c) 20 A, and (d) 25 A
- Fig. 4.42 RS-PMSM-WPB (a) airgap flux density plot, (b) back EMFs curves and (b) harmonic spectrum
- Fig. 4.43 Variation of (a) stator hysteresis loss, (b) rotor hysteresis loss, (c) stator eddy-current loss, (d) rotor eddy-current loss, (e) PM eddy-current loss, and (f) copper loss with current angle, δ , and peak current, I_m
- Fig. 5.1 Presented double-stage PV array fed PMSM drive based water pumping system with the provision to deliver power to local loads
- Fig. 5.2 Conventional double-stage PV array fed PMSM drive based water pumping system
- Fig. 5.3 Presented single-stage solar PV array fed PMSM drive based water pumping system with the provision to deliver power to local loads

- Fig. 5.4 Conventional single-stage PV array fed PMSM drive based water pumping system
- Fig. 5.5 Illustration of basic concept behind incremental conductance based MPPT algorithm
- Fig. 5.6 Flowchart of incremental conductance based MPPT algorithm
- Fig. 5.7 Pictorial representation of actual and observed rotor flux in PMSM
- Fig. 5.8 (a) Pure integrator based estimation of rotor flux, and (b) Bode curve of pure integrator
- Fig. 5.9 (a) LPF based observation of rotor flux, and (b) Bode curve of LPF
- Fig. 5.10 ANF based observation of rotor flux
- Fig. 5.11 Bode curve of ANF
- Fig. 5.12 Improved ANF based observation of rotor flux
- Fig. 5.13 Bode curve of improved ANF
- Fig. 5.14 Bode curve of $G_e(s)$ at $\omega_e=314\text{rad/s}$, $3\omega_e$, $5\omega_e$, and $7\omega_e$
- Fig. 5.15 Presented AMNF based observation of rotor flux
- Fig. 5.16 Bode curve of presented AMNF structure
- Fig. 5.17 Bode curves of presented AMNF structure and existing filters
- Fig. 5.18 Flux loci of (a) Pure integrator, (b) LPF, (c) ANF, (b) IANF and (c) presented AMNF structure under DC disturbance
- Fig. 5.19 Flux loci of (a) Pure integrator, (b) LPF, (c) ANF, (d) IANF and (e) presented AMNF structure under harmonic disturbance
- Fig. 5.20 Control for generation of switching pulses for motor-side VSI
- Fig. 5.21 Control for generation of switching pulses for load-side VSC
- Fig. 5.22 Flowchart of incremental conductance based MPPT algorithm
- Fig. 5.23 MATLAB/Simulink based model of double-stage solar PV array fed PMSM drive with local loads for water pumping system
- Fig. 5.24 MATLAB/Simulink based model of single-stage solar PV array fed PMSM drive with local loads for water pumping system
- Fig. 5.25 Experimental setup
- Fig. 5.26 (a) Schematic diagram of signal conditioning circuit for voltage sensors, and (b) voltage sensor board as developed in laboratory
- Fig. 5.27 (a) Schematic diagram of signal conditioning circuit for current sensors, and (b) current sensor board as developed in laboratory
- Fig. 5.28 (a) Schematic diagram of isolation and amplification circuit for gate drivers, and (b) optocoupler based isolation and BJT based amplification board as developed in laboratory

- Fig. 5.29 (a) Architecture of dSPACE-1202 based DSP, and (b) photograph of dSPACE-1202
- Fig. 5.30 Starting and steady-state performances of double-stage PV array fed PMSM driven water pumping system at 1kW/m^2 . (a) PV array/load parameters, and (b) PMSM parameters
- Fig. 5.31 Starting and steady-state performances of double-stage PV array fed PMSM driven water pumping system at 0.5kW/m^2 . (a) PV array/load parameters, and (b) PMSM parameters
- Fig. 5.32 Dynamic performances of presented double-stage PV array fed PMSM driven water pumping system for irradiation change from 1kW/m^2 to 0.5kW/m^2 . (a) PV array/local-load parameters, and (b) PMSM parameters
- Fig. 5.33 Dynamic performances of presented double-stage PV array fed PMSM driven water pumping system for irradiation change from 0.5kW/m^2 to 1kW/m^2 . (a) PV array/local-load parameters, and (b) PMSM parameters
- Fig. 5.34 Starting performances of presented double-stage PV array fed PMSM driven water pumping system at (a,c) 1kW/m^2 , and (b,d) 0.5kW/m^2
- Fig. 5.35 Steady-state performances of presented double-stage PV array fed PMSM driven water pumping system at (a-e) 1kW/m^2 , and (f-i) 0.5kW/m^2
- Fig. 5.36 Dynamic performances of presented double-stage PV array fed PMSM driven water pumping system for irradiation change from 0.5kW/m^2 to 1kW/m^2 . (a) $\hat{\omega}_{me}, \hat{\phi}_{mr}, \hat{\phi}_{m\alpha}, \hat{\phi}_{m\beta}$; (b) $I_{PV}, i_{ma}, i_{mb}, i_{mc}$; (c) $P_{PV}, V_{PV}, I_{PV}, V_{DC}$; (d) I_{PV}, i_{ma}, v_L, i_L and (e) $\hat{\omega}_{me}, V_{DC}, i_{ma}, \hat{\theta}_{me}$
- Fig. 5.37 Dynamic performances of presented double-stage PV array fed PMSM driven water pumping system for irradiation change from 1kW/m^2 to 0.5kW/m^2 . (a) $\hat{\omega}_{me}, \hat{\phi}_{mr}, \hat{\phi}_{m\alpha}, \hat{\phi}_{m\beta}$; (b) $I_{PV}, i_{ma}, i_{mb}, i_{mc}$; (c) $P_{PV}, V_{PV}, I_{PV}, V_{DC}$; (d) I_{PV}, i_{ma}, v_L, i_L and (e) $\hat{\omega}_{me}, V_{DC}, i_{ma}, \hat{\theta}_{me}$
- Fig. 5.38 Illustration of MPPT performance on I_{PV} -vs- V_{PV} curve for presented double-stage PV array fed water pumping system at (a) 1kW/m^2 , and (b) 0.5kW/m^2
- Fig. 5.39 Starting and steady-state performances of single-stage PV array fed PMSM driven water pumping system at 1kW/m^2 . (a) PV array/load parameters, and (b) PMSM parameters
- Fig. 5.40 Starting and steady-state performances of single-stage PV array fed PMSM driven water pumping system at 0.5kW/m^2 . (a) PV array/load parameters, and (b) PMSM parameters
- Fig. 5.41 Dynamic performances of presented single-stage PV array fed PMSM driven water pumping system for irradiation change from 1kW/m^2 to 0.5kW/m^2 . (a) PV array/local-load parameters, and (b) PMSM parameters
- Fig. 5.42 Dynamic performances of presented single-stage PV array fed PMSM driven water pumping system for irradiation change from 0.5kW/m^2 to 1kW/m^2 . (a) PV array/local-load parameters, and (b) PMSM parameters

- Fig. 5.43 Starting performances of presented single-stage PV array fed PMSM driven water pumping system at (a-b) 1kW/m^2 , and (c-d) 0.5kW/m^2
- Fig. 5.44 Steady-state performances of presented single-stage PV array fed PMSM driven water pumping system at (a-d) 1kW/m^2 , and (e-h) 0.5kW/m^2
- Fig. 5.45 Dynamic performances of presented single-stage PV array fed PMSM driven water pumping system for irradiation change from (a-d) 0.5kW/m^2 to 1kW/m^2 , and (e-h) vice-versa
- Fig. 5.46 Illustration of MPPT performance on I_{PV} -vs- V_{PV} curve for presented single-stage PV array fed water pumping system at (a) 1kW/m^2 , and (b) 0.5kW/m^2
- Fig. 6.1 Double-stage solar PV array and BES fed PMSM-pumping system with local loads
- Fig. 6.2 Double-stage solar PV array and BES with BDC fed PMSM-pumping system with local loads
- Fig. 6.3 Single-stage solar PV array and BES with bidirectional converter fed PMSM-pumping system with local loads
- Fig. 6.4 Control of bidirectional converter for double stage system
- Fig. 6.5 Control of bidirectional converter for single-stage system
- Fig. 6.6 MATLAB/Simulink based model of double-stage solar PV array and battery fed PMSM drive with local loads for water pumping system
- Fig. 6.7 MATLAB/Simulink based model of double-stage solar PV array and battery with bidirectional DC-DC converter fed PMSM drive with local loads for water pumping system
- Fig. 6.8 MATLAB/Simulink based model of single-stage solar PV array and battery with bidirectional DC-DC converter fed PMSM drive with local loads for water pumping system
- Fig. 6.9 Experimental setup
- Fig. 6.10 Starting and steady-state performances of double-stage PV array and battery fed PMSM drive with local-loads for water pumping system at 1 kW/m^2
- Fig. 6.11 Starting and steady-state performances of double-stage PV array and battery fed PMSM drive with local-loads for water pumping system at 0.5 kW/m^2
- Fig. 6.12 Dynamic performances of presented double-stage PV array and battery fed PMSM drive with local-loads for water pumping system for irradiation change from $\{1\text{-to-}0.5\}\text{kW/m}^2$
- Fig. 6.13 Dynamic performances of double-stage PV array and battery fed PMSM drive with local-loads for water pumping system for irradiation change from $\{0.5\text{-to-}1.0\}\text{kW/m}^2$
- Fig. 6.14 Performances of presented double-stage PV array and battery fed PMSM drive with local-loads for water pumping system during shut-down of pumping unit at 1kW/m^2
- Fig. 6.15 Performances of presented double-stage PV array and battery fed PMSM drive with local-loads for water pumping system during shut-down of pumping unit at 0.5 kW/m^2

- Fig. 6.16 Starting performances of double-stage PV array and battery fed PMSM drive with local-loads for water pumping system at irradiation of (a,c) 1.0 kW/m^2 , and (b,d) 0 kW/m^2
- Fig. 6.17 Steady-state performances of double-stage PV array and battery fed PMSM drive with local-loads for water pumping system at irradiation of (a-c) 1 kW/m^2 , and (d-f) 0.5 kW/m^2
- Fig. 6.18 Dynamic performances of double-stage PV array and battery fed PMSM drive with local-loads for water pumping system for change in irradiation from (a-d) $\{0.5\text{-to-}1.0\} \text{ kW/m}^2$, and (e-h) vice-versa
- Fig. 6.19 Dynamic performances of double-stage PV array and battery fed PMSM drive with local-loads for water pumping system for change in irradiation from (a-c) $\{0.0\text{-to-}1.0\} \text{ kW/m}^2$, and (d-f) vice-versa
- Fig. 6.20 Dynamic performances of presented system for irradiation change from (a) $\{0.5\text{-to-}1.0\} \text{ kW/m}^2$, and (b) vice-versa when pumping is not required
- Fig. 6.21 Illustration of MPPT performance on $I_{PV}\text{-vs-}V_{PV}$ curve for presented double-stage PV array and battery fed water pumping system at (a) 1kW/m^2 , and (b) 0.5kW/m^2
- Fig. 6.22 Starting and steady-state performances of double-stage PV array and battery with bidirectional converter fed PMSM drive with local-loads for water pumping system at 1 kW/m^2
- Fig. 6.23 Starting and steady-state performances of double-stage PV array and BES with BDC fed PMSM drive with local-loads for water pumping system at 0.5 kW/m^2
- Fig. 6.24 Dynamic performances of double-stage PV array and BES with BDC fed PMSM drive with local-loads for water pumping system for irradiation change from $\{1\text{-to-}0.5\} \text{ kW/m}^2$
- Fig. 6.25 Dynamic performances of double-stage PV array and BES with BDC fed PMSM drive with local-loads for water pumping system for irradiation change from $\{0.5\text{-to-}1\} \text{ kW/m}^2$
- Fig. 6.26 Performances of presented double-stage PV array and BES with BDC fed PMSM drive with local-loads for water pumping system during shut-down of pumping unit at 1kW/m^2
- Fig. 6.27 Performances of double-stage PV array and BES with BDC fed PMSM drive with local-loads for water pumping system during shut-down of pumping unit at 0.5kW/m^2
- Fig. 6.28 Starting performances of presented double-stage PV array and battery with BDC fed PMSM driven water pumping system at solar irradiation of (a) 1.0kW/m^2 , and (b) 0.0kW/m^2
- Fig. 6.29 Steady-state performances of presented double-stage PV array and battery with BDC fed PMSM driven water pumping system at irradiation of (a,c) 1kW/m^2 , and (b,d) 0.5kW/m^2
- Fig. 6.30 Dynamic performances of presented double-stage PV array and battery with BDC fed PMSM driven water pumping system for irradiation change from (a-c) $\{0.0\text{-to-}1.0\}\text{kW/m}^2$, and (d-f) vice-versa

- Fig. 6.31 Dynamic performances of presented double-stage PV array and battery with BDC fed PMSM driven water pumping system for irradiation change from (a-d) $\{0.5\text{-to-}1.0\}$ kW/m², and (e-h) vice-versa
- Fig. 6.32 Dynamic performances of presented system for irradiation change from (a) $\{0.5\text{-to-}1.0\}$ kW/m², and (b) vice-versa when pumping is not required
- Fig. 6.33 Illustration of MPPT performance on $I_{PV}\text{-vs-}V_{PV}$ curve for presented double-stage PV array and BES with BDC fed water pumping system at (a) 1kW/m², and (b) 0.5kW/m²
- Fig. 6.34 Starting and steady-state performances of single-stage PV array and battery with bidirectional converter fed PMSM driven water pumping system at 1.0 kW/m²
- Fig. 6.35 Starting and steady-state performances of single-stage PV array and battery with bidirectional converter fed PMSM driven water pumping system at 0.5 kW/m²
- Fig. 6.36 Dynamic performances of single-stage PV array and BES with BDC fed PMSM driven water pumping system for irradiation change from $\{1\text{-to-}0.5\}$ kW/m²
- Fig. 6.37 Dynamic performances of single-stage PV array and BES with BDC fed PMSM driven water pumping system for irradiation change from $\{0.5\text{-to-}1.0\}$ kW/m²
- Fig. 6.38 Performances of presented single-stage PV array and BES with BDC fed PMSM driven water pumping system during shut-down of pumping unit at 1kW/m²
- Fig. 6.39 Performances of presented single-stage PV array and BES with BDC fed PMSM driven water pumping system during shut-down of pumping unit at 0.5kW/m²
- Fig. 6.40 Starting performances of presented single-stage PV array and battery with BDC fed PMSM driven water pumping system at irradiation of (a,c) 0kW/m², and (b,d) 1kW/m²
- Fig. 6.41 Steady-state performances of presented single-stage PV array and battery with BDC fed PMSM driven water pumping system at irradiation of (a-c) 1kW/m², and (d-f) 0.5kW/m²
- Fig. 6.42 Dynamic performances of single-stage PV array and BES with BDC fed PMSM driven system for irradiation change from (a-d) $\{0.5\text{-to-}1.0\}$ kW/m², and (e-h) vice-versa
- Fig. 6.43 Dynamic performances of presented single-stage PV array and battery with BDC fed PMSM driven water pumping system for irradiation change from (a-d) $\{0.0\text{-to-}1.0\}$ kW/m², and (e-h) vice-versa
- Fig. 6.44 Dynamic performances of presented system for irradiation change from (a) $\{0.5\text{-to-}1.0\}$ kW/m², and (b) vice-versa when pumping is not required
- Fig. 6.45 Illustration of MPPT performance on $I_{PV}\text{-vs-}V_{PV}$ curve for presented single-stage PV array and BES with BDC fed water pumping system at (a) 1kW/m², and (b) 0.5kW/m²
- Fig. 7.1 Single-phase grid-interfaced double-stage solar PV array fed PMSM drive with local-loads for water pumping system
- Fig. 7.2 Single-phase grid-synchronized single-stage solar PV array fed PMSM drive with local-loads for water pumping system
- Fig. 7.3 Control scheme based on presented AMNF-FLL for generation of switching pulses for grid-side VSC

- Fig. 7.4 Block diagram of ANF-FLL
- Fig. 7.5 Frequency response of ANF structure
- Fig. 7.6 Frequency response of $G_e(s)$ at $\omega_{ct}=314\text{rad/s}$, $5\omega_{ct}$, and $7\omega_{ct}$
- Fig. 7.7 Block diagram of presented AMNF-FLL structure
- Fig. 7.8 Frequency response of (a) $G_{AMNFp}(s)$, and (b) $G_{AMNFq}(s)$
- Fig. 7.9 Control for generation of switching pulses for motor-side VSI
- Fig. 7.10 AMNF-FLL based voltage control scheme for generation of switching pulses for grid-side VSC during islanded-mode
- Fig. 7.11 (a) AMNF-FLL based seamless control to synchronize water pumping system with grid, and (b) Control for matching phase-angle and frequency of load voltage with the phase-angle and frequency of grid-voltage
- Fig. 7.12 MATLAB/Simulink based model of single-phase grid-interfaced double-stage solar PV array fed PMSM drive with local loads for water pumping system
- Fig. 7.13 MATLAB/Simulink based model of single-phase grid-synchronized single-stage solar PV array fed PMSM drive with local-loads for water pumping system
- Fig. 7.14 Experimental setup
- Fig. 7.15 Starting and steady-state performances of (a) G , I_{PV} , V_{PV} , P_{PV} , V_{DC} , and (b) i_{abcm} , ω_m , θ_e , v_L , i_L when PV array alone feeding the system
- Fig. 7.16 Steady-state performances of (a) v_g , i_g , i_L , u_p , w_T , (b) P_g , V_{DC} , i_{abcm} , ω_m , θ_e , and (c) THD of i_g when grid alone feeding the system
- Fig. 7.17 Steady-state performances of (a) G , I_{PV} , V_{PV} , v_g , i_g , (b) w_T , i_L , i_{abcm} , ω_m , θ_e , and (c) THD of i_g when both the PV array and grid feeding the system
- Fig. 7.18 Steady-state performances of (a) G , I_{PV} , V_{PV} , v_g , i_g , (b) w_T , u_p , i_L , V_{DC} , ω_m , and (c) THD of i_g when PV array feeding the utility grid
- Fig. 7.19 Dynamic performances of (a) G , I_{PV} , V_{PV} , v_g , i_g , (b) w_T , i_L , i_{abcm} , ω_m , θ_e , and (c) THD of i_g for transition from PV array alone feeding the system to grid alone feeding the system
- Fig. 7.20 Dynamic performances of (a) G , I_{PV} , V_{PV} , v_g , i_g , (b) w_T , i_L , i_{abcm} , ω_m , θ_e , and (c) THD of i_g for transition from PV array alone feeding to both the PV array and grid feeding the system
- Fig. 7.21 Dynamic performances of (a) G , I_{PV} , V_{PV} , v_g , i_g , (b) w_T , u_p , i_L , V_{DC} , ω_m , and (c) THD of i_g when PV array feeding the utility grid for change in irradiation from (1.0-to-0.5) kW/m^2
- Fig. 7.22 Performance curves of v_g , i_g , w_T , u_p , ω_m , during (a) voltage sag, and (b) recovery from voltage sag when grid alone feeding the system along with (c) THD in i_g
- Fig. 7.23 Performance curves of v_g , i_g , w_T , u_p , ω_m , during (a) voltage swell, and (b) recovery from voltage swell when grid alone feeding the system along with (c) THD in i_g

- Fig. 7.24 Starting and steady-state performances when solar PV array alone feeding the system (irradiation is 1.0kW/m^2). Profiles of (a) ω_{me} , i_{ma} , I_{PV} , w_{Tg} , (b) P_{PV} , P_g , θ_{me} , i_L (c) v_g , I_{PV} , i_g , i_L , (d) i_g , I_{PV} , i_{ma} , i_L , and (e) ω_{me} , I_{PV} , θ_{me} , i_{ma}
- Fig. 7.25 Starting and steady-state performances when both utility grid and PV array feeding the system (irradiation is 0.5kW/m^2). Profiles of (a) ω_{me} , i_{ma} , I_{PV} , w_{Tg} , (b) P_{PV} , P_g , θ_{me} , i_L , (c) v_g , I_{PV} , i_g , i_L , (d) i_g , I_{PV} , i_{ma} , i_L , and (e) ω_{me} , I_{PV} , θ_{me} , i_{ma}
- Fig. 7.26 Steady-state performances when grid alone feeding the system (irradiation is 0kW/m^2). Profiles of (a) v_g , I_{PV} , i_g , i_L , and (b) i_g , I_{PV} , i_{ma} , i_L
- Fig. 7.27 Steady-state behavior when PV array feeding grid at (a) 1kW/m^2 , and (b) 0.5kW/m^2
- Fig. 7.28 MPPT performances of PV array at (a) 1.0kW/m^2 , and (b) 0.5kW/m^2
- Fig. 7.29 Dynamic performances of system for transition from (a-b) PV alone feeding the system to grid alone feeding the system, and (c-d) vice-versa
- Fig. 7.30 Dynamic performances of system for change in irradiation from (a-d) $\{1.0\text{-to-}0.5\}\text{kW/m}^2$, and (e-h) vice-versa
- Fig. 7.31 Dynamic performances when PV array feeding grid for change in irradiation from (a) $\{1.0\text{-to-}0.5\}\text{kW/m}^2$, and (b) vice-versa
- Fig. 7.32 Performance of grid parameters under (a,c) voltage sag, and (b,d) recovery from voltage sag at (a-b) 0.5kW/m^2 , and (c-d) 0kW/m^2
- Fig. 7.33 Performance of grid parameters under (a,c) voltage swell, and (b,d) recovery from voltage swell at (a-b) 0.5kW/m^2 , and (c-d) 0.0kW/m^2
- Fig. 7.34 Performance of grid parameters under voltage distortion. Profiles of (a) v_g , $v_{g\alpha}$, i_g , ω_{me} , and (b) $v_{g\alpha}\text{-vs-}v_{g\beta}$
- Fig. 7.35 Power quality performances when grid alone feeding the system under (a-d) normal operation, (e-h) voltage sag and (i-l) voltage swell
- Fig. 7.36 Power quality performances when grid alone feeding system under voltage distortion. (a) v_g , i_g , (b) P_g , (c) fundamental component of v_g , (d) 3rd harmonic of v_g , (e) 5th harmonic of v_g , (f) 7th harmonic of v_g , (g) fundamental component of i_g , (h) 3rd harmonic of i_g , (i) 5th harmonic of i_g , and (j) 7th harmonic of i_g
- Fig. 7.37 Starting and steady-state performances of (a,c) G , I_{PV} , V_{PV} , v_g , i_g , w_T , and (b,d) $i_{abc m}$, ω_m , θ_e , v_L , i_L , u_p under GCM at constant irradiation of (a-b) 1 kW/m^2 , and (c-d) 0.5 kW/m^2
- Fig. 7.38 Dynamic performances of (a,c) G , I_{PV} , V_{PV} , v_g , i_g , w_T , and (b,d) $i_{abc m}$, ω_m , θ_e , v_L , i_L , u_p under GCM for change in irradiation from (a-b) $1.0\text{kW/m}^2\text{-to-}0.5\text{kW/m}^2$, and (c-d) vice-versa
- Fig. 7.39 Starting and steady-state performances of (a,c) G , I_{PV} , V_{PV} , v_g , i_g , w_T , and (b,d) $i_{abc m}$, ω_m , θ_e , v_L , i_L , u_p under IDM at constant irradiation of (a-b) 1 kW/m^2 , and (c-d) 0.5 kW/m^2
- Fig. 7.40 Dynamic performances of (a,c) G , I_{PV} , V_{PV} , v_g , i_g , w_T , and (b,d) $i_{abc m}$, ω_m , θ_e , v_L , i_L , u_p under IDM for change in irradiation from (a-b) $1.0\text{kW/m}^2\text{-to-}0.5\text{kW/m}^2$, and (c-d) vice-versa

- Fig. 7.41 Performances of (a,c) $v_g, i_g, T_{syn}, \theta_e, V_{pv}$, and (b,d) $v_L, i_L, v_{gp}, e_{\theta}, u_p$ for changeover from (a-b) grid connected mode to islanded mode, and (c-d) vice-versa
- Fig. 7.42 Starting performances of system under GCM at (a,c) 1.0kW/m^2 , and (b,d) 0.5kW/m^2
- Fig. 7.43 Steady-state performances under GCM at (a-c) 1kW/m^2 , and (d-f) 0.5kW/m^2
- Fig. 7.44 MPPT performances of PV array at (a) 1kW/m^2 , and (b) 0.5kW/m^2
- Fig. 7.45 Power quality performances under GCM at (a-g) 0kW/m^2 , and (h-n) 0.5kW/m^2
- Fig. 7.46 Dynamic performances of system under GCM for change in irradiation from (a-d) $\{1.0\text{-to-}0.5\}\text{kW/m}^2$, and (e-h) vice-versa
- Fig. 7.47 Starting performances of system under IDM at (a,c) 1.0kW/m^2 , and (b,d) 0.5kW/m^2
- Fig. 7.48 Steady-state performances under IDM at (a-b) 1kW/m^2 , and (c-d) 0.5kW/m^2
- Fig. 7.49 Dynamic performances of system under IDM for change in irradiation from (a-b) $\{1.0\text{-to-}0.5\}\text{kW/m}^2$, and (c-d) vice-versa
- Fig. 7.50 Performances of system for seamless mode transition from (a-d) GCM-to-IDM, and (e-h) IDM-to-GCM.
- Fig. 8.1 Single-phase grid-interfaced double-stage solar PV array and BES fed PMSM drive for water pumping system
- Fig. 8.2 Single-phase grid-interfaced double-stage solar PV array and BES with bidirectional converter fed PMSM drive for water pumping system
- Fig. 8.3 Single-phase grid-interfaced single-stage solar PV array and BES with bidirectional converter fed PMSM drive for water pumping system
- Fig. 8.4 Single-phase grid-interfaced double-stage solar PV array and BES fed PMSM drive with local-loads for water pumping system
- Fig. 8.5 Single-phase grid-interfaced double-stage solar PV array and BES with bidirectional converter fed PMSM drive with local loads for water pumping system
- Fig. 8.6 Single-phase grid-synchronized single-stage solar PV array and BES with bidirectional converter fed PMSM drive with local-loads for water pumping system
- Fig. 8.7 MATLAB/Simulink based model of single-phase grid-interfaced double-stage solar PV array and BES fed PMSM drive for water pumping system
- Fig. 8.8 MATLAB/Simulink based model of single-phase grid-interfaced double-stage solar PV array and BES with bidirectional converter fed PMSM drive for water pumping system
- Fig. 8.9 MATLAB/Simulink based model of single-phase grid-interfaced single-stage solar PV array and BES with bidirectional converter fed PMSM drive for water pumping system
- Fig. 8.10 MATLAB/Simulink based model of single-phase grid-interfaced double-stage solar PV array and BES fed PMSM drive with local-loads for water pumping system

- Fig. 8.11 MATLAB/Simulink based model of single-phase grid-interfaced double-stage solar PV array and BES with BDC fed PMSM drive with local loads for water pumping system
- Fig. 8.12 MATLAB/Simulink based model of single-phase grid-synchronized single-stage solar PV array and BES with BDC fed PMSM drive with local-loads for water pumping system
- Fig. 8.13 Experimental setup
- Fig. 8.14 Starting and steady-state performances of G , V_{PV} , I_{PV} , i_g , v_g , i_{abc} , ω_m , θ_e at (a) 1kW/m^2 , and (b) 0.5kW/m^2 when grid is available along with (c) THD in i_g at 0.5kW/m^2
- Fig. 8.15 Dynamic performances of (a) G , V_{PV} , I_{PV} , P_{PV} , V_{DC} , v_g , i_g , and (b) u_p , ω_m , i_{abc} , θ_e , P_{pmsm} , I_q for change in irradiation from 1kW/m^2 to 0.5kW/m^2 when grid is available
- Fig. 8.16 Performance curves of v_g , i_g , u_p , ω_m , during (a) voltage sag, and (b) voltage swell at solar irradiation of 0.0kW/m^2 along with (c) THD in i_g
- Fig. 8.17 Starting and steady-state performances of G , V_{PV} , I_{PV} , V_{BES} , I_{BES} , i_{abc} , ω_m , θ_e at (a) 1kW/m^2 , and (b) 0.5kW/m^2 when grid is not available
- Fig. 8.18 Dynamic performances of (a) G , V_{PV} , I_{PV} , P_{PV} , V_{DC} , v_g , P_{BES} , and (b) V_{BES} , I_{BES} , i_{abc} , ω_m , θ_e , P_{pmsm} , I_q for change in irradiation from 1kW/m^2 to 0.5kW/m^2 when grid is not available
- Fig. 8.19 Starting [(a),(d)] and steady-state [(b)-(c), (e)-(f)] performances of system at (a-c) 1kW/m^2 , and (d-f) 0.5kW/m^2 when water pumping is required in the presence of utility grid
- Fig. 8.20 Steady-state performance of system at (a) 1kW/m^2 , and (b) 0.5kW/m^2 when water pumping is not required in the presence of utility grid
- Fig. 8.21 MPPT performances of PV array at (a) 1.0kW/m^2 , and (b) 0.5kW/m^2
- Fig. 8.22 Performance of (a) I_{PV} , v_g , i_g , i_{ma} , (b) V_{DC} , P_{PV} , P_g , P_{inv} , and (c) V_{PV} , I_{PV} , P_{PV} , i_g during dynamics of solar irradiation when water pumping is required in the presence of utility grid
- Fig. 8.23 Performance of (a) V_{DC} , P_{PV} , P_g , P_{inv} , and (c-d) I_{PV} , v_g , i_g , i_{ma} , during dynamics of solar irradiation when water pumping is not required in the presence of utility grid
- Fig. 8.24 Performance of ω_{me} , v_g , i_g , ω_{tg} under (a-b) voltage sag, and (c-d) voltage swell at solar irradiation of (a,c) 0kW/m^2 and (b,d) 0.5kW/m^2
- Fig. 8.25 Performance of grid parameters under voltage distortion. Profiles of (a) v_g , $v_{g\alpha}$, i_g , ω_{me} , and (b) $v_{g\alpha}$ -vs- $v_{g\beta}$
- Fig. 8.26 Power quality performances under (a-d) normal operation, (e-h) voltage sag and (i-l) voltage swell
- Fig. 8.27 Power quality performances under voltage distortion. (a) v_g , i_g , (b) P_g , (c) fundamental component of v_g , (d) v_g : 3rd harmonic (e) v_g : 5th harmonic, (f) v_g : 7th harmonic, (g) fundamental component of i_g , (h) 3rd harmonic of i_g , (i) 5th harmonic of i_g , and (j) 7th harmonic of i_g

- Fig. 8.28 Starting [(a),(d)] and steady-state [(b)-(c), (e)-(f)] performances of system at (a-c) 1kW/m^2 , and (d-f) 0.5kW/m^2 when water pumping is required in the absence of utility grid
- Fig. 8.29 Performance of (a) I_{PV} , V_{BES} , I_{BES} , i_{ma} , and (b) V_{DC} , P_{PV} , V_{PV} , I_{PV} during dynamics of solar irradiation when water pumping is required in the absence of utility grid
- Fig. 8.30 Performance of (a) I_{PV} , V_{BES} , I_{BES} , i_{ma} , and (b) V_{DC} , P_{PV} , P_{inv} , P_g during dynamics of solar irradiation when water pumping is not required in the absence of utility grid
- Fig. 8.31 Starting and steady-state performances of I_{PV} , V_{PV} , I_{BES} , V_{BES} , v_g , i_g , i_{abcm} , ω_m , at (a) 1kW/m^2 , and (b) 0.5kW/m^2 when grid is available along with (c) THD in i_g
- Fig. 8.32 Dynamic performances of (a) G , V_{PV} , I_{PV} , P_{PV} , V_{DC} , V_{BES} , I_{BES} , P_{BES} , and (b) v_g , i_g , u_p , w_T , i_{abcm} , ω_m , θ_e , P_{pmsm} for change in irradiation from (1.0-to-0.5) kW/m^2 when grid is available
- Fig. 8.33 Performance curves of v_g , i_g , u_p , w_T , ω_m , during (a) voltage sag, and (b) voltage swell at solar irradiation of 0.0kW/m^2 along with (c) THD in i_g
- Fig. 8.34 Starting and steady-state performances of G , V_{PV} , I_{PV} , V_{BES} , I_{BES} , v_g , i_{abcm} , ω_m , at (a) 1kW/m^2 , and (b) 0.5kW/m^2 when grid is not available
- Fig. 8.35 Dynamic performances of (a) G , V_{PV} , I_{PV} , P_{PV} , V_{DC} , V_{BES} , I_{BES} , P_{BES} , and (b) v_g , i_g , w_T , i_{abcm} , ω_m , θ_e , P_{pmsm} , I_q for change in irradiation from (1-to-0.5) kW/m^2 when grid is not available
- Fig. 8.36 Starting [(a),(d)] and steady-state [(b)-(c), (e)-(f)] performances of system at (a-c) 1kW/m^2 , and (d-f) 0.5kW/m^2 when water pumping is required in the presence of utility grid
- Fig. 8.37 Steady-state performance of system at (a) 1kW/m^2 , and (b) 0.5kW/m^2 when water pumping is not required in the presence of utility grid
- Fig. 8.38 MPPT performances of PV array at (a) 1.0kW/m^2 , and (b) 0.5kW/m^2
- Fig. 8.39 Performance of (a,c) i_g , P_{BES} , V_{BES} , I_{BES} , and (b,d) V_{PV} , I_{PV} , P_{PV} , i_g during dynamics of solar irradiation when water pumping is required in the presence of utility grid
- Fig. 8.40 Performance of I_{PV} , v_g , i_g , i_{ma} , during dynamics of solar irradiation from (a) (1-to-0.5) kW/m^2 and (b) vice-versa, when water pumping is not required in the presence of grid
- Fig. 8.41 Performance of ω_{me} , w_{tg} , i_g , v_g under (a) voltage sag, (b) recovery from voltage sag, (c) voltage swell and (d) recovery from voltage swell
- Fig. 8.42 Performance of grid parameters under voltage distortion. Profiles of (a) v_g , $v_{g\alpha}$, i_g , ω_{me} , and (b) $v_{g\alpha}$ -vs- $v_{g\beta}$
- Fig. 8.43 Power quality performances, under (a-d) normal operation, (e-h) voltage sag and (i-l) voltage swell
- Fig. 8.44 Power quality performances under voltage distortion. (a) v_g , i_g , (b) P_g , (c) fundamental component of v_g , (d) v_g : 3rd harmonic, (e) v_g : 5th harmonic, (f) v_g : 7th harmonic, (g) fundamental component of i_g , (h) 3rd harmonic of i_g , (i) 5th harmonic of i_g , and (j) 7th harmonic of i_g

- Fig. 8.45 Starting [(a),(c)] and steady-state [(b), (d)] performances of system at (a-b) 1kW/m^2 , and (c-d) 0.5kW/m^2 when water pumping is required in the absence of utility grid
- Fig. 8.46 Performance of (a,c) P_{BES} , V_{DC} , I_{PV} , V_{BES} , and (b) V_{DC} , P_{PV} , V_{PV} , I_{PV} during dynamics of solar irradiation when water pumping is required in the absence of utility grid
- Fig. 8.47 Performance of P_{BES} , V_{DC} , I_{BES} , V_{BES} during dynamics of solar irradiation from (a) (1-to-0.5) kW/m^2 and (b) vice-versa when water pumping is not required in the absence of grid
- Fig. 8.48 Starting and steady-state performances of I_{PV} , V_{PV} , I_{BES} , V_{BES} , v_g , i_g , i_{abcm} , ω_m , at (a) 1kW/m^2 , and (b) 0.5kW/m^2 when grid is available along with (c) THD in i_g
- Fig. 8.49 Dynamic performances of (a) G , V_{PV} , I_{PV} , P_{PV} , V_{DC} , V_{BES} , I_{BES} , P_{BES} , and (b) v_g , i_g , u_p , w_T , i_{abcm} , ω_m , θ_e , P_{pmsm} for change in irradiation from (1.0-to-0.5) kW/m^2 when grid is available
- Fig. 8.50 Performance curves of v_g , i_g , u_p , w_T , ω_m , during (a) voltage sag, and (b) voltage swell at solar irradiation of 0.0kW/m^2 along with (c) THD in i_g
- Fig. 8.51 Starting and steady-state performances of G , V_{PV} , I_{PV} , V_{BES} , I_{BES} , v_g , i_{abcm} , ω_m , at (a) 1kW/m^2 , and (b) 0.5kW/m^2 when grid is not available
- Fig. 8.52 Dynamic performances of (a) G , V_{PV} , I_{PV} , P_{PV} , V_{DC} , V_{BES} , I_{BES} , P_{BES} , and (b) v_g , i_g , w_T , i_{abcm} , ω_m , θ_e , P_{pmsm} , I_q for change in irradiation from (1-to-0.5) kW/m^2 when grid is not available
- Fig. 8.53 Starting [(a),(d)] and steady-state [(b)-(c), (e)-(f)] performances of system at (a-c) 1kW/m^2 , and (d-f) 0.5kW/m^2 when water pumping is required in the presence of utility grid
- Fig. 8.54 Steady-state performance of system at (a) 1kW/m^2 , and (b) 0.5kW/m^2 when water pumping is not required in the presence of utility grid
- Fig. 8.55 MPPT performances of PV array at (a) 1.0kW/m^2 , and (b) 0.5kW/m^2
- Fig. 8.56 Dynamic performance of system for change in irradiation from (a-c) $\{1.0\text{-to-}0.5\}\text{kW/m}^2$, and (d-f) vice-versa, when water pumping is required in the presence of utility grid
- Fig. 8.57 Performance of V_{DC} , I_{PV} , v_g , i_g during dynamics of solar irradiation from (a) (1-to-0.5) kW/m^2 and (b) vice-versa when water pumping is not required in the presence of grid
- Fig. 8.58 Performance of ω_{me} , w_{Tg} , i_g , v_g under (a-b) voltage sag, and (c-d) voltage swell at solar irradiation of (a,c) 0kW/m^2 , and (b,d) 0.5kW/m^2
- Fig. 8.59 Performance of grid parameters under voltage distortion. Profiles of (a) v_g , $v_{g\alpha}$, i_g , ω_{me} , and (b) $v_{g\alpha}$ -vs- $v_{g\beta}$
- Fig. 8.60 Power quality performances under (a-d) normal operation, (e-h) voltage sag and (i-l) voltage swell
- Fig. 8.61 Power quality performances under voltage distortion. (a) v_g , i_g , (b) P_g , (c) fundamental component of v_g , (d) 3rd harmonic of v_g , (e) 5th harmonic of v_g , (f) 7th harmonic of v_g , (g) fundamental component of i_g , (h) 3rd harmonic of i_g , (i) 5th harmonic of i_g , and (j) 7th harmonic of i_g

- Fig. 8.62 Starting [(a),(d)] and steady-state [(b)-(c), (e)-(f)] performances of system at (a-c) 1kW/m^2 , and (d-f) 0.5kW/m^2 when water pumping is required in the absence of grid
- Fig. 8.63 Performance of (a) i_{ma} , I_{BES} , I_{PV} , V_{PV} , and (b) P_{BES} , V_{PV} , I_{BES} , V_{BES} during dynamics of solar irradiation when water pumping is required in the absence of utility grid
- Fig. 8.64 Performance of P_{PV} , I_{PV} , I_{BES} , P_{BES} during dynamics of solar irradiation from (a) (1-to-0.5) kW/m^2 and (b) vice-versa when water pumping is not required in the absence of grid
- Fig. 8.65 Starting and steady-state performances of G , V_{PV} , I_{PV} , v_g , i_g , i_L , i_{abcm} , ω_m , at (a) 1kW/m^2 , and (b) 0.5kW/m^2 when grid is available along with (c) THD in i_g at 0.5kW/m^2
- Fig. 8.66 Dynamic performances of (a) G , V_{PV} , I_{PV} , P_{PV} , V_{DC} , u_p , w_T , and (b) v_g , i_g , i_L , i_{abcm} , ω_m , θ_e , I_q for change in irradiation from 1kW/m^2 to 0.5kW/m^2 when grid is available
- Fig. 8.67 Performance curves of v_g , i_g , u_p , w_T , ω_m , during (a) voltage sag, and (b) voltage swell at solar irradiation of 0.0kW/m^2 along with (c) THD in i_g
- Fig. 8.68 Starting and steady-state performances of V_{PV} , I_{PV} , V_{BES} , I_{BES} , v_L , i_L , i_{abcm} , ω_m , at (a) 1kW/m^2 , and (b) 0.5kW/m^2 when grid is not available
- Fig. 8.69 Dynamic performances of (a) G , V_{PV} , I_{PV} , P_{PV} , V_{DC} , v_L , i_L , and (b) V_{BES} , I_{BES} , P_{BES} , i_{abcm} , ω_m , θ_e , I_q for change in irradiation from 1kW/m^2 to 0.5kW/m^2 when grid is not available
- Fig. 8.70 Starting [(a),(d)] and steady-state [(b)-(c), (e)-(f)] performances of system at (a-c) 1kW/m^2 , and (d-f) 0.5kW/m^2 when water pumping is required in the presence of utility grid
- Fig. 8.71 Steady-state performance of system at (a) 1kW/m^2 , and (b) 0.5kW/m^2 when water pumping is not required in the presence of utility grid
- Fig. 8.72 MPPT performances of PV array at (a) 1.0kW/m^2 , and (b) 0.5kW/m^2
- Fig. 8.73 Performance of (a,c) v_g , I_{PV} , i_g , i_L , and (b,d) V_{PV} , P_{PV} , V_{DC} , I_{PV} during dynamics of solar irradiation when water pumping is required in the presence of utility grid
- Fig. 8.74 Performance of v_g , I_{PV} , i_g , i_L , during dynamics of solar irradiation from (a) (1-to-0.5) kW/m^2 and (b) vice-versa when water pumping is not required in the presence of grid
- Fig. 8.75 Performance of v_g , i_g , w_{Tg} , ω_{me} under (a) voltage sag, and (b) voltage swell
- Fig. 8.76 Performance of grid parameters under voltage distortion. Profiles of (a) v_g , $v_{g\alpha}$, i_g , ω_{me} , and (b) $v_{g\alpha}$ -vs- $v_{g\beta}$
- Fig. 8.77 Power quality performances under (a-d) normal operation, (e-h) voltage sag and (i-l) voltage swell
- Fig. 8.78 Power quality performances under voltage distortion. (a) v_g , i_g , (b) P_g , (c) fundamental component of v_g , (d) 3rd harmonic of v_g , (e) 5th harmonic of v_g , (f) 7th harmonic of v_g , (g) fundamental component of i_g , (h) 3rd harmonic of i_g , (i) 5th harmonic of i_g , and (j) 7th harmonic of i_g

- Fig. 8.79 Starting [(a),(d)] and steady-state [(b)-(c), (e)-(f)] performances of system at (a-c) 1kW/m^2 , and (d-f) 0.5kW/m^2 when water pumping is required in the absence of grid
- Fig. 8.80 Performance of (a,c) V_{DC} , I_{PV} , v_L , i_L , (b) ω_{me} , I_{BES} , i_{ma} , θ_{me} , and (c) P_{PV} , V_{DC} , I_{PV} , V_{PV} , during dynamics of solar irradiation when water pumping is required in the absence of grid
- Fig. 8.81 Performance of I_{BES} , I_{PV} , i_{ma} , i_L during dynamics of solar irradiation from (a) (1-to-0.5) kW/m^2 and (b) vice-versa when water pumping is not required in the absence of grid
- Fig. 8.82 Starting and steady-state performances of I_{PV} , V_{PV} , I_{BES} , V_{BES} , v_g , i_g , i_L , ω_m , at (a) 1kW/m^2 , and (b) 0.5kW/m^2 when grid is available along with (c) THD in i_g
- Fig. 8.83 Dynamic performances of (a) G , V_{PV} , I_{PV} , P_{PV} , V_{DC} , V_{BES} , I_{BES} , P_{BES} , and (b) v_g , i_g , i_L , u_p , w_T , i_{abcm} , ω_m , θ_e , for change in irradiation from (1.0-to-0.5) kW/m^2 when grid is available
- Fig. 8.84 Performance curves of v_g , i_g , u_p , w_T , ω_m , during (a) voltage sag, and (b) voltage swell at solar irradiation of 0.0kW/m^2 along with (c) THD in i_g
- Fig. 8.85 Starting and steady-state performances of V_{PV} , I_{PV} , V_{BES} , I_{BES} , v_L , i_L , i_{abcm} , ω_m , at (a) 1kW/m^2 , and (b) 0.5kW/m^2 when grid is not available
- Fig. 8.86 Dynamic performances of (a) G , V_{PV} , I_{PV} , P_{PV} , V_{DC} , v_L , i_L , and (b) V_{BES} , I_{BES} , P_{BES} , i_{abcm} , ω_m , θ_e , I_q for change in irradiation from (1-to-0.5) kW/m^2 when grid is not available
- Fig. 8.87 Starting [(a),(e)] and steady-state [(b)-(d), (f)-(h)] performances of system at (a-c) 1kW/m^2 , and (d-f) 0.5kW/m^2 when utility grid is available
- Fig. 8.88 MPPT performances of PV array at (a) 1.0kW/m^2 , and (b) 0.5kW/m^2
- Fig. 8.89 Dynamic performance of system for change in irradiation from (a)-(c) {1.0-to-0.5} kW/m^2 , and (d-f) vice-versa, when utility grid is available
- Fig. 8.90 Performance of ω_{me} , w_{Tg} , i_g , v_g under (a) voltage sag, (b) voltage swell
- Fig. 8.91 Performance of grid parameters under voltage distortion. Profiles of (a) v_g , $v_{g\alpha}$, i_g , ω_{me} , and (b) $v_{g\alpha}$ -vs- $v_{g\beta}$
- Fig. 8.92 Power quality performances under (a-d) normal operation, (e-h) voltage sag and (i-l) voltage swell
- Fig. 8.93 Power quality performances under voltage distortion. (a) v_g , i_g , (b) P_g , (c) fundamental component of v_g , (d) v_g : 3rd harmonic, (e) v_g : 5th harmonic, (f) v_g : 7th harmonic, (g) fundamental component of i_g , (h) 3rd harmonic of i_g , (i) 5th harmonic of i_g , and (j) 7th harmonic of i_g
- Fig. 8.94 Starting [(a),(d)] and steady-state [(b)-(c), (e)-(f)] performances of system at (a-c) 1kW/m^2 , and (d-f) 0.5kW/m^2 when utility grid is not available
- Fig. 8.95 Performance of (a) V_{DC} , I_{PV} , I_{BES} , V_{BES} , (b) P_{PV} , V_{DC} , I_{PV} , V_{PV} , and (c) P_{PV} , i_{ma} , i_{mb} , i_{mc} during dynamics of solar irradiation when utility grid is not available
- Fig. 8.96 Starting and steady-state performances of I_{PV} , V_{PV} , I_{BES} , V_{BES} , v_g , i_g , i_L , ω_m under GCM at (a) 1kW/m^2 , and (b) 0.5kW/m^2

- Fig. 8.97 Dynamic performances of (a) $G, I_{PV}, V_{PV}, P_{PV}, I_{BES}, V_{BES}, P_{BES}$, and (b) $v_g, i_g, i_L, u_p, w_T, i_{abc}, \omega_m, \theta_e$ under GCM for change in irradiation from $\{1.0\text{-to-}0.5\}$ kW/m²
- Fig. 8.98 Starting and steady-state performances of $I_{PV}, V_{PV}, I_{BES}, V_{BES}, v_g, i_g, v_L, i_L, \omega_m$ under IDM at (a) 1kW/m², and (b) 0.5kW/m²
- Fig. 8.99 Dynamic performances of (a) $G, V_{PV}, I_{PV}, P_{PV}, V_{BES}, I_{BES}, P_{BES}$, and (b) $v_g, i_g, v_L, i_L, i_{abc}, \omega_m, \theta_e$ under IDM for change in irradiation from $\{1.0\text{-to-}0.5\}$ kW/m²
- Fig. 8.100 Performances of (a) $T_{syn}, \theta_g, \theta_L, e_\theta, V_{pv}, u_p$, and (b) $v_g, i_g, v_L, i_L, v_{gp}$ for changeover from grid connected mode to islanded mode
- Fig. 8.101 Performances of (a) $T_{syn}, \theta_g, \theta_L, e_\theta, V_{pv}, u_p$, and (b) $v_g, i_g, v_L, i_L, v_{gp}$ for changeover from islanded mode to grid connected mode
- Fig. 8.102 MPPT performances of PV array at (a) 1.0kW/m², and (b) 0.5kW/m²
- Fig. 8.103 Steady-state performances under GCM at (a-c) 1kW/m², and (d-f) 0.5kW/m²
- Fig. 8.104 Dynamic performances of system under GCM for change in irradiation from (a-c) $\{1.0\text{-to-}0.5\}$ kW/m², and (d-f) vice-versa
- Fig. 8.105 Steady-state performances under IDM at (a-c) 1kW/m², and (d-f) 0.5kW/m²
- Fig. 8.106 Dynamic performances of system under IDM for change in irradiation from (a-c) $\{1.0\text{-to-}0.5\}$ kW/m², and (d-f) vice-versa
- Fig. 8.107 Performances of system for seamless mode transition from (a-d) GCM-to-IDM, and (e-h) IDM-to-GCM.
- Fig. 9.1 Three-phase grid-interfaced double-stage solar PV array fed PMSM drive with local-loads for water pumping system
- Fig. 9.2 Three-phase grid-synchronized single-stage solar PV array fed PMSM drive with local-loads for water pumping system
- Fig. 9.3 Control scheme based on AMNF-FLL for generation of switching pulses for grid VSC
- Fig. 9.4 Voltage control scheme for generation of switching pulses for grid-side VSC under islanded-mode
- Fig. 9.5 Presented AMNF-FLL based synchronization scheme
- Fig. 9.6 Angle and frequency matching controller
- Fig. 9.7 MATLAB/Simulink based model of three-phase grid-interfaced double-stage solar PV array fed PMSM drive with local loads for water pumping system
- Fig. 9.8 MATLAB/Simulink based model of three-phase grid-synchronized single-stage solar PV array fed PMSM drive with local-loads for water pumping system
- Fig. 9.9 Starting and steady-state performances of (a) $G, I_{PV}, V_{PV}, P_{PV}, V_{DC}$, and (b) $i_{abc}, \omega_m, \theta_e, v_{Labc}, i_{Labc}$ when PV array alone feeding the system
- Fig. 9.10 Steady-state performances of (a) $v_{gabc}, i_{gabc}, i_{Labc}, u_{pa}, w_T$, (b) $P_g, V_{DC}, i_{abc}, \omega_m, \theta_e$, and (c) THD of i_{ga} when grid alone feeding the system
- Fig. 9.11 Steady-state performances of (a) $G, I_{PV}, V_{PV}, v_{gabc}, i_{gabc}$, (b) $w_T, i_{Labc}, i_{abc}, \omega_m, \theta_e$, and (c) THD of i_{ga} when both the PV array and grid feeding the system

- Fig. 9.12 Steady-state performances of (a) $G, I_{PV}, V_{PV}, v_{gabc}, i_{gabc}$, (b) $W_T, u_{pa}, i_{Labc}, V_{DC}, \omega_m$, and (c) THD of i_{ga} when PV array feeding the utility grid
- Fig. 9.13 Dynamic performances of (a) $G, I_{PV}, V_{PV}, v_{gabc}, i_{gabc}$, (b) $W_T, i_{Labc}, i_{abcm}, \omega_m, \theta_e$, and (c) THD of i_{ga} for transition from PV array alone feeding system to grid alone feeding the system
- Fig. 9.14 Dynamic performances of (a) $G, I_{PV}, V_{PV}, v_{gabc}, i_{gabc}$, (b) $W_T, i_{Labc}, i_{abcm}, \omega_m, \theta_e$, and (c) THD of i_{ga} for transition from PV array alone feeding to both PV array and grid feeding system
- Fig. 9.15 Dynamic performances of (a) $G, I_{PV}, V_{PV}, v_{gabc}, i_{gabc}$, (b) $W_T, u_{pa}, i_{Labc}, V_{DC}, \omega_m$, and (c) THD of i_{ga} when PV array feeding grid for change in irradiation from (1.0-to-0.5) kW/m^2
- Fig. 9.16 Performance curves of (a-b) $v_{gabc}, i_{gabc}, W_T, u_{pa}, \omega_m$, during (a) voltage sag, and (b) voltage swell when grid alone feeding the system along with (c) THD in i_g under voltage sag, and (d) THD in i_g under voltage swell
- Fig. 9.17 Starting performance of the system when solar PV array alone feeding the system (irradiation is 1.0kW/m^2). Profiles of (a) $\omega_{me}, I_{PV}, \theta_{me}, i_{ma}$, and (b) $i_{ma}, \theta_{me}, W_T, i_L$
- Fig. 9.18 Steady-state performance of system when solar PV array alone feeding the system (irradiation is 1.0kW/m^2). Profiles of (a) $v_{ga}, v_{gb}, v_{gc}, i_{ga}$, (b) $v_{ga}, i_{ga}, i_{gb}, i_{gc}$, (c) $I_{PV}, i_g, i_{ma}, i_{La}$, (d) i_{ma}, v_g, i_g, i_{La} , and (e) $\omega_{me}, I_{PV}, \theta_{me}, i_{ma}$
- Fig. 9.19 Starting performance of the system when both PV array and grid feeding the system (irradiation is 0.5kW/m^2). Profiles of (a) $\omega_{me}, I_{PV}, \theta_{me}, i_{ma}$, and (b) $i_{ma}, \theta_{me}, W_T, i_{La}$
- Fig. 9.20 Steady-state performance of system when solar PV array alone feeding the system (irradiation is 1.0kW/m^2). Profiles of (a) $v_{ga}, v_{gb}, v_{gc}, i_{ga}$, (b) $v_{ga}, i_{ga}, i_{gb}, i_{gc}$, (c) $I_{PV}, i_g, i_{ma}, i_{La}$, (d) i_{ma}, v_g, i_g, i_{La} , and (e) $\omega_{me}, I_{PV}, \theta_{me}, i_{ma}$
- Fig. 9.21 Steady-state performance of system when grid alone feeding the system (irradiation is 0.0kW/m^2). Profiles of (a) $v_{ga}, v_{gb}, v_{gc}, i_{ga}$, (b) $v_{ga}, i_{ga}, i_{gb}, i_{gc}$, (c) $v_{ga}, i_{La}, i_{Lb}, i_{Lc}$, (d) $I_{PV}, i_g, i_{ma}, i_{La}$, (e) i_{ma}, v_g, i_g, i_{La} , and (f) $\omega_{me}, I_{PV}, \theta_{me}, i_{ma}$
- Fig. 9.22 Steady-state performances when solar PV array feeding the utility grid at (a-b) 1kW/m^2 , and (c-d) 0.5kW/m^2
- Fig. 9.23 MPPT performances of PV array (a) 1.0kW/m^2 , and (b) 0.5kW/m^2
- Fig. 9.24 Dynamic performances of system for transition from (a-c) PV alone feeding the system to grid alone feeding the system, and (d-f) vice-versa
- Fig. 9.25 Dynamic performances of system for change in irradiation from (a-d) $\{1.0\text{-to-}0.5\}\text{kW/m}^2$, and (e-h) vice-versa
- Fig. 9.26 Dynamic performances when PV array feeding grid for change in irradiation from (a-b) $\{1.0\text{-to-}0.5\}\text{kW/m}^2$, and (c-d) vice-versa
- Fig. 9.27 Performances under (a,c) voltage sag, and (b,d) recovery from voltage sag
- Fig. 9.28 Performances under (a,c) voltage swell, and (b,d) recovery from voltage swell
- Fig. 9.29 Power quality performances when grid alone feeding the system under (a-d) normal operation, (e-h) voltage sag and (i-l) voltage swell

- Fig. 9.30 Power quality performances at 500 W/m^2 under (a-d) normal operation, (e-h) voltage sag and (i-l) voltage swell
- Fig. 9.31 Starting and steady-state performances of (a,c) $G, I_{PV}, V_{PV}, v_{gabc}, i_{gabc}, w_T$, and (b,d) $i_{abc}, \omega_m, \theta_e, v_{Labc}, i_{Labc}, u_{pa}$ under GCM at irradiation of (a-b) 1 kW/m^2 , and (c-d) 0.5 kW/m^2
- Fig. 9.32 Dynamic performances of (a,c) $G, I_{PV}, V_{PV}, v_{gabc}, i_{gabc}, w_T$, and (b,d) $i_{abc}, \omega_m, \theta_e, v_{Labc}, i_{Labc}, u_{pa}$ under GCM for irradiation change from (a-b) $\{1\text{-to-}0.5\} \text{ kW/m}^2$, and (c-d) vice-versa
- Fig. 9.33 Starting and steady-state performances of (a,c) $G, I_{PV}, V_{PV}, v_{gabc}, i_{gabc}, w_T$, and (b,d) $i_{abc}, \omega_m, \theta_e, v_{Labc}, i_{Labc}, u_{pa}$ for IDM at steady irradiation of (a-b) 1 kW/m^2 , and (c-d) 0.5 kW/m^2
- Fig. 9.34 Dynamic performances of (a,c) $G, I_{PV}, V_{PV}, v_{gabc}, i_{gabc}, w_T$, and (b,d) $i_{abc}, \omega_m, \theta_e, v_{Labc}, i_{Labc}, u_{pa}$ for IDM for irradiation change from (a-b) $1 \text{ kW/m}^2\text{-to-}0.5 \text{ kW/m}^2$, and (c-d) vice-versa
- Fig. 9.35 Performances of (a,c) $v_{ga}, i_{ga}, T_{syn}, \theta_e, V_{pv}$, and (b,d) $v_{La}, i_{La}, v_{gp}, e_{\theta}, u_{pa}$ for changeover from (a-b) grid connected mode to islanded mode, and (c-d) vice-versa
- Fig. 9.36 Starting performances of system under GCM at (a-b) 1.0 kW/m^2 , and (c-d) 0.5 kW/m^2
- Fig. 9.37 Steady-state performances under GCM at 1 kW/m^2
- Fig. 9.38 Steady-state performances under GCM at 0.5 kW/m^2
- Fig. 9.39 MPPT performances of PV array at (a) 1 kW/m^2 , and (b) 0.5 kW/m^2
- Fig. 9.40 Power quality performances under GCM at (a-d) 0 kW/m^2 , and (e-h) 0.5 kW/m^2
- Fig. 9.41 Dynamic performances under GCM for change in irradiation from $\{1\text{-to-}0.5\} \text{ kW/m}^2$
- Fig. 9.42 Dynamic performances under GCM for change in irradiation from $\{0.5\text{-to-}1\} \text{ kW/m}^2$
- Fig. 9.43 Starting performances of system under IDM at (a,c) 1.0 kW/m^2 , and (b,d) 0.5 kW/m^2
- Fig. 9.44 Steady-state performances under IDM at (a-d) 1 kW/m^2 , and (e-h) 0.5 kW/m^2
- Fig. 9.45 Dynamic performances of system under IDM for change in irradiation from (a-d) $\{1.0\text{-to-}0.5\} \text{ kW/m}^2$, and (e-h) vice-versa
- Fig. 9.46 Performances of system for seamless mode transition from (a-d) GCM-to-IDM, and (e-h) IDM-to-GCM.
- Fig. 10.1 Three-phase grid-interfaced double-stage solar PV array and BES fed PMSM drive for water pumping system
- Fig. 10.2 Three-phase grid-interfaced double-stage solar PV array and BES with bidirectional converter fed PMSM drive for water pumping system
- Fig. 10.3 Three-phase grid-interfaced single-stage solar PV array and BES with bidirectional converter fed PMSM drive for water pumping system
- Fig. 10.4 Three-phase grid-interfaced double-stage solar PV array and BES fed PMSM drive with local-loads for water pumping system

- Fig. 10.5 Three-phase grid-interfaced double-stage solar PV array and BES with bidirectional converter fed PMSM drive with local loads for water pumping system
- Fig. 10.6 Three-phase grid-synchronized single-stage PV array and BES with bidirectional converter fed PMSM drive with local-loads for water pumping system
- Fig. 10.7 MATLAB/Simulink based model of three-phase grid-interfaced double-stage solar PV array and BES fed PMSM drive for water pumping system
- Fig. 10.8 MATLAB/Simulink based model of three-phase grid-interfaced double-stage solar PV array and BES with BDC fed PMSM drive for water pumping system
- Fig. 10.9 MATLAB/Simulink based model of three-phase grid-interfaced single-stage solar PV array and BES with BDC fed PMSM drive for water pumping system
- Fig. 10.10 MATLAB/Simulink based model of three-phase grid-interfaced double-stage solar PV array and BES fed PMSM drive with local-loads for water pumping system
- Fig. 10.11 MATLAB/Simulink based model of three-phase grid-interfaced double-stage solar PV array and BES with BDC fed PMSM drive with local loads for water pumping system
- Fig. 10.12 MATLAB/Simulink based model of three-phase grid-synchronized single-stage solar PV array and BES with BDC fed PMSM drive with local-loads for water pumping system
- Fig. 10.13 Experimental setup
- Fig. 10.14 Starting and steady-state performances of G , V_{PV} , I_{PV} , i_g , v_g , i_{abc} , ω_m , θ_e at (a) 1kW/m^2 , and (b) 0.5kW/m^2 when grid is available along with (c) THD in i_g at 0.5kW/m^2
- Fig. 10.15 Dynamic performances of (a) G , V_{PV} , I_{PV} , P_{PV} , V_{DC} , v_g , i_g , and (b) u_p , ω_T , i_{abc} , ω_m , θ_e , P_{pmsm} , I_q for change in irradiation from 1kW/m^2 to 0.5kW/m^2 when grid is available
- Fig. 10.16 Performance curves of v_g , i_g , u_p , ω_T , ω_m , during (a) voltage sag, and (b) voltage swell at solar irradiation of 0.0kW/m^2 along with (c) THD in i_g
- Fig. 10.17 Starting and steady-state performances of G , V_{PV} , I_{PV} , V_{BES} , I_{BES} , i_{abc} , ω_m , θ_e at (a) 1kW/m^2 , and (b) 0.5kW/m^2 when grid is not available
- Fig. 10.18 Dynamic performances of (a) G , V_{PV} , I_{PV} , P_{PV} , V_{DC} , v_g , P_{BES} , and (b) V_{BES} , I_{BES} , i_{abc} , ω_m , θ_e , P_{pmsm} , I_q for change in irradiation from 1kW/m^2 to 0.5kW/m^2 when grid is not available
- Fig. 10.19 Starting [(a),(d)] and steady-state [(b)-(c), (e)-(h)] performances of system at (a-c) 1kW/m^2 , and (d-h) 0.5kW/m^2 when water pumping is required in the presence of utility grid
- Fig. 10.20 Steady-state performance of system at (a) 1kW/m^2 , and (b) 0.5kW/m^2 when water pumping is not required in the presence of utility grid
- Fig. 10.21 MPPT performances of PV array at (a) 1.0kW/m^2 , and (b) 0.5kW/m^2
- Fig. 10.22 Performance of (a) P_{PV} , V_{PV} , I_{PV} , i_{ga} , and (b) I_{PV} , v_g , i_g , i_{ma} , during dynamics of solar irradiation when water pumping is required in the presence of utility grid

- Fig. 10.23 Performance of (a-b) P_{PV} , V_{DC} , P_g , P_{inv} , and (c-d) I_{PV} , v_{ga} , i_{ga} , i_{ma} , during dynamics of solar irradiation when water pumping is not required in the presence of utility grid
- Fig. 10.24 Performance of v_{ga} , i_{ga} , ω_{me} under (a-b) voltage sag, and (c-d) voltage swell at solar irradiation of (a,c) 0kW/m^2 and (b,d) 0.5kW/m^2
- Fig. 10.25 Power quality performances of system under (a-d) normal operation, (e-h) voltage sag and (i-l) voltage swell
- Fig. 10.26 Starting [(a-b),(c-d)] and steady-state [(c), (f)] performances of system at (a-c) 1kW/m^2 , and (d-f) 0.5kW/m^2 when water pumping is required in the absence of grid
- Fig. 10.27 Performance of (a) P_{PV} , V_{DC} , I_{PV} , V_{PV} , and (b-c) V_{BES} , I_{BES} , I_{PV} , i_{ma} during dynamics of solar irradiation when water pumping is required in the absence of utility grid
- Fig. 10.28 Performance of (a) V_{DC} , P_{PV} , P_g , P_{inv} , and (a) V_{BES} , I_{BES} , I_{PV} , i_{ma} during dynamics of solar irradiation when water pumping is not required in the absence of utility grid
- Fig. 10.29 Starting and steady-state performances of I_{PV} , V_{PV} , I_{BES} , V_{BES} , v_g , i_g , i_{abcm} , ω_m , at (a) 1kW/m^2 , and (b) 0.5kW/m^2 when grid is available along with (c) THD in i_g
- Fig. 10.30 Dynamic performances of (a) G , V_{PV} , I_{PV} , P_{PV} , V_{DC} , V_{BES} , I_{BES} , P_{BES} , and (b) v_g , i_g , u_p , ω_m , θ_e , P_{pmsm} for change in irradiation from $(1.0\text{-to-}0.5)\text{kW/m}^2$ when grid is available
- Fig. 10.31 Performance curves of v_g , i_g , u_p , ω_m , during (a) voltage sag, and (b) voltage swell at solar irradiation of 0.0kW/m^2 along with (c) THD in i_g
- Fig. 10.32 Starting and steady-state performances of G , V_{PV} , I_{PV} , V_{BES} , I_{BES} , v_g , i_{abcm} , ω_m , at (a) 1kW/m^2 , and (b) 0.5kW/m^2 when grid is not available
- Fig. 10.33 Dynamic performances of (a) G , V_{PV} , I_{PV} , P_{PV} , V_{DC} , V_{BES} , I_{BES} , P_{BES} , and (b) v_g , i_g , ω_m , θ_e , P_{pmsm} , I_q for change in irradiation from $(1\text{-to-}0.5)\text{kW/m}^2$ when grid is not available
- Fig. 10.34 Starting [(a),(e)] and steady-state [(b)-(d), (f)-(h)] performances of system at (a-c) 1kW/m^2 , and (d-f) 0.5kW/m^2 when water pumping is required in the presence of utility grid
- Fig. 10.35 Steady-state performance of system at (a) 1kW/m^2 , and (b) 0.5kW/m^2 when water pumping is not required in the presence of utility grid
- Fig. 10.36 MPPT performances of PV array at (a) 1.0kW/m^2 , and (b) 0.5kW/m^2
- Fig. 10.37 Performance of (a,c) P_{PV} , V_{PV} , I_{PV} , i_{ga} and (b,d) i_{ma} , I_{PV} , v_{ga} , i_{ga} during dynamics of solar irradiation when water pumping is required in the presence of utility grid
- Fig. 10.38 Performance of i_{ma} , I_{PV} , v_{ga} , i_{ga} , during dynamics of solar irradiation from (a) $(1\text{-to-}0.5)\text{kW/m}^2$ and (b) vice-versa, when water pumping is not required in the presence of utility grid
- Fig. 10.39 Performance of ω_{me} , ω_{tg} , i_{ga} , v_{ga} under (a) voltage sag, (b) recovery from voltage sag, (c) voltage swell and (d) recovery from voltage swell
- Fig. 10.40 Power quality performances of system under (a-d) normal operation, (e-h) voltage sag and (i-l) voltage swell

- Fig. 10.41 Starting [(a),(c)] and steady-state [(b), (d)] performances of system at (a-b) $1\text{kW}/\text{m}^2$, and (c-d) $0.5\text{kW}/\text{m}^2$ when water pumping is required in the absence of utility grid
- Fig. 10.42 Performance of (a,d) P_{BES} , V_{DC} , V_{BES} , I_{BES} , (b,e) P_{PV} , V_{DC} , I_{PV} , V_{PV} and (c,f) ω_{me} , θ_{me} , I_{PV} , i_{ma} during dynamics of irradiation when water pumping is required in the absence of grid
- Fig. 10.43 Performance of P_{PV} , I_{PV} , P_{BES} , I_{BES} during dynamics of solar irradiation from (a) (1-to-0.5) kW/m^2 and (b) vice-versa when water pumping is not required in the absence of grid
- Fig. 10.44 Starting and steady-state performances of I_{PV} , V_{PV} , I_{BES} , V_{BES} , v_g , i_g , i_{abcm} , ω_m , at (a) $1\text{kW}/\text{m}^2$, and (b) $0.5\text{kW}/\text{m}^2$ when grid is available along with (c) THD in i_g
- Fig. 10.45 Dynamic performances of (a) G , V_{PV} , I_{PV} , P_{PV} , V_{DC} , V_{BES} , I_{BES} , P_{BES} , and (b) v_g , i_g , u_p , w_T , i_{abcm} , ω_m , θ_e , P_{pmsm} for change in irradiation from (1-to-0.5) kW/m^2 when grid is available
- Fig. 10.46 Performance curves of v_g , i_g , u_p , w_T , ω_m , during (a) voltage sag, and (b) voltage swell at solar irradiation of $0.0\text{kW}/\text{m}^2$ along with (c) THD in i_g
- Fig. 10.47 Starting and steady-state performances of G , V_{PV} , I_{PV} , V_{BES} , I_{BES} , v_g , i_{abcm} , ω_m , at (a) $1\text{kW}/\text{m}^2$, and (b) $0.5\text{kW}/\text{m}^2$ when grid is not available
- Fig. 10.48 Dynamic performances of (a) G , V_{PV} , I_{PV} , P_{PV} , V_{DC} , V_{BES} , I_{BES} , P_{BES} , and (b) v_g , i_g , w_T , i_{abcm} , ω_m , θ_e , P_{pmsm} , I_q for change in irradiation from (1-to-0.5) kW/m^2 when grid is not available
- Fig. 10.49 Starting [(a),(d)] and steady-state [(b)-(c), (e)-(h)] performances of system at (a-d) $1\text{kW}/\text{m}^2$, and (e-h) $0.5\text{kW}/\text{m}^2$ when water pumping is required in the presence of utility grid
- Fig. 10.50 Steady-state performance of system at (a) $1\text{kW}/\text{m}^2$, and (b) $0.5\text{kW}/\text{m}^2$ when water pumping is not required in the presence of utility grid
- Fig. 10.51 MPPT performances of PV array at (a) $1.0\text{kW}/\text{m}^2$, and (b) $0.5\text{kW}/\text{m}^2$
- Fig. 10.52 Performance of (a) i_{ma} , I_{PV} , v_{ga} , i_{ga} , and (b) V_{DC} , I_{PV} , I_{BES} , i_{ga} during dynamics of solar irradiation when water pumping is required in the presence of utility grid
- Fig. 10.53 Performance of (a,c) i_{ma} , I_{PV} , v_{ga} , i_{ga} , and (b,d) w_{Tg} , I_{PV} , I_{BES} , i_{ma} during dynamics of solar irradiation from (a-b) $\{1\text{-to-}0.5\}\text{kW}/\text{m}^2$ and (c-d) vice-versa when water pumping is not required in the presence of grid
- Fig. 10.54 Performance of ω_{me} , w_{Tg} , i_{ga} , v_{ga} under (a-b) voltage sag, and (c-d) voltage swell at solar irradiation of (a,c) $0\text{kW}/\text{m}^2$, and (b,d) $0.5\text{kW}/\text{m}^2$
- Fig. 10.55 Power quality performances of system under (a-d) normal operation, (e-h) voltage sag and (i-l) voltage swell
- Fig. 10.56 Starting [(a),(d)] and steady-state [(b)-(c), (e)-(f)] performances of system at (a-c) $1\text{kW}/\text{m}^2$, and (d-f) $0.5\text{kW}/\text{m}^2$ when water pumping is required in the absence of grid
- Fig. 10.57 Performance of (a-b) V_{PV} , I_{PV} , I_{BES} , i_{ma} , and (c) P_{PV} , I_{PV} , P_{BES} , I_{BES} during dynamics of solar irradiation when water pumping is required in the absence of utility grid
- Fig. 10.58 Performance of (a-b) P_{PV} , I_{PV} , P_{BES} , I_{BES} , and (c) V_{PV} , I_{PV} , I_{BES} , i_{ma} during dynamics of solar irradiation from when water pumping is not required in the absence of grid

- Fig. 10.59 Starting and steady-state performances of G , V_{PV} , I_{PV} , v_g , i_g , i_L , i_{abcm} , ω_m , at (a) 1kW/m^2 , and (b) 0.5kW/m^2 when grid is available along with (c) THD in i_g at 0.5kW/m^2
- Fig. 10.60 Dynamic performances of (a) G , V_{PV} , I_{PV} , P_{PV} , V_{DC} , u_p , w_T , and (b) v_g , i_g , i_L , i_{abcm} , ω_m , θ_e , I_q for change in irradiation from 1kW/m^2 to 0.5kW/m^2 when grid is available
- Fig. 10.61 Performance curves of v_g , i_g , u_p , w_T , ω_m , during (a) voltage sag, and (b) voltage swell at solar irradiation of 0.0kW/m^2 along with (c) THD in i_g
- Fig. 10.62 Starting and steady-state performances of V_{PV} , I_{PV} , V_{BES} , I_{BES} , v_L , i_L , i_{abcm} , ω_m , at (a) 1kW/m^2 , and (b) 0.5kW/m^2 when grid is not available
- Fig. 10.63 Dynamic performances of (a) G , V_{PV} , I_{PV} , P_{PV} , V_{DC} , v_L , i_L , and (b) V_{BES} , I_{BES} , P_{BES} , i_{abcm} , ω_m , θ_e , I_q for change in irradiation from 1kW/m^2 to 0.5kW/m^2 when grid is not available
- Fig. 10.64 Starting [(a),(e)] and steady-state [(b)-(d), (f)-(i)] performances of system at (a-d) 1kW/m^2 , and (e-i) 0.5kW/m^2 when water pumping is required in the presence of grid
- Fig. 10.65 Steady-state performance of system at (a) 1kW/m^2 , and (b) 0.5kW/m^2 when water pumping is not required in the presence of utility grid
- Fig. 10.66 MPPT performances of PV array at (a) 1.0kW/m^2 , and (b) 0.5kW/m^2
- Fig. 10.67 Performance of (a) v_{ga} , i_{ma} , i_{ga} , i_{La} , (b) P_{PV} , V_{DC} , V_{PV} , I_{PV} , (c) I_{PV} , i_{ga} , i_{ma} , i_{La} , and (d) ω_{me} , I_{PV} , θ_{me} , i_{ma} during dynamics of solar irradiation when water pumping is required in the presence of utility grid
- Fig. 10.68 Performance of i_{ma} , v_{ga} , i_{ga} , i_{La} , during dynamics of solar irradiation from (a) (1-to- 0.5) kW/m^2 and (b) vice-versa when water pumping is not required in the presence of grid
- Fig. 10.69 Performance of ω_{me} , w_{Tg} , i_g , v_g , under (a) voltage sag, and (b) voltage swell
- Fig. 10.70 Power quality performances for (a-d) normal operation, (e-h) sag and (i-l) swell
- Fig. 10.71 Starting [(a),(d)] and steady-state [(b)-(c), (e)-(h)] performances of system at (a-c) 1kW/m^2 , and (d-h) 0.5kW/m^2 when water pumping is required in the absence of utility grid
- Fig. 10.72 Performance of (a) V_{DC} , I_{PV} , v_{La} , i_{La} , (b) P_{PV} , V_{DC} , I_{PV} , V_{PV} , and (c) I_{PV} , I_{BES} , i_{ma} , i_{La} during dynamics of solar irradiation when water pumping is required in the absence of grid
- Fig. 10.73 Performance of I_{PV} , I_{BES} , i_{ma} , i_{La} during dynamics of solar irradiation from (a) $\{1\text{-to-}0.5\}$ kW/m^2 and (b) vice-versa when water pumping is not required in the absence of grid
- Fig. 10.74 Starting and steady-state performances of I_{PV} , V_{PV} , I_{BES} , V_{BES} , v_g , i_g , i_L , ω_m , at (a) 1kW/m^2 , and (b) 0.5kW/m^2 when grid is available along with (c) THD in i_g
- Fig. 10.75 Dynamic performances of (a) G , V_{PV} , I_{PV} , P_{PV} , V_{DC} , V_{BES} , I_{BES} , P_{BES} , and (b) v_g , i_g , i_L , u_p , w_T , i_{abcm} , ω_m , θ_e , for change in irradiation from (1.0-to- 0.5) kW/m^2 when grid is available

- Fig. 10.76 Performance curves of v_g , i_g , u_p , w_T , ω_m , during (a) voltage sag, and (b) voltage swell at solar irradiation of 0.0kW/m^2 along with (c) THD in i_g
- Fig. 10.77 Starting and steady-state performances of V_{PV} , I_{PV} , V_{BES} , I_{BES} , v_L , i_L , i_{abcm} , ω_m , at (a) 1kW/m^2 , and (b) 0.5kW/m^2 when grid is not available
- Fig. 10.78 Dynamic performances of (a) G , V_{PV} , I_{PV} , P_{PV} , V_{DC} , v_L , i_L , and (b) V_{BES} , I_{BES} , P_{BES} , i_{abcm} , ω_m , θ_e , I_q for change in irradiation from (1-to-0.5) kW/m^2 when grid is not available
- Fig. 10.79 Starting [(a),(e)] and steady-state [(b)-(d), (f)-(h)] performances of system at (a-d) 1kW/m^2 , and (e-h) 0.5kW/m^2 when utility grid is available
- Fig. 10.80 MPPT performances of PV array at (a) 1.0kW/m^2 , and (b) 0.5kW/m^2
- Fig. 10.81 Dynamic performance of system for change in irradiation from (a-c) $\{1.0\text{-to-}0.5\}$ kW/m^2 , and (d-f) vice-versa, when utility grid is available
- Fig. 10.82 Power quality performances at solar irradiation of (a) 1kW/m^2 , and (b) 0.5kW/m^2
- Fig. 10.83 Starting [(a),(e)] and steady-state [(b)-(d), (f)-(h)] performances of system at (a-d) 1kW/m^2 , and (f-h) 0.5kW/m^2 when utility grid is not available
- Fig. 10.84 Performance of (a,d) i_{La} , v_{La} , V_{BES} , I_{BES} , (b,e) V_{DC} , I_{PV} , I_{BES} , i_{ma} , and (c,f) V_{PV} , I_{PV} , V_{DC} , P_{PV} during dynamics of solar irradiation when utility grid is not available
- Fig. 10.85 Starting and steady-state performances of I_{PV} , V_{PV} , I_{BES} , V_{BES} , v_g , i_g , i_L , ω_m under GCM at (a) 1kW/m^2 , and (b) 0.5kW/m^2
- Fig. 10.86 Dynamic performances of (a) G , I_{PV} , V_{PV} , P_{PV} , I_{BES} , V_{BES} , P_{BES} , and (b) v_g , i_g , i_L , u_p , w_T , i_{abcm} , ω_m , θ_e under GCM for change in irradiation from $\{1.0\text{-to-}0.5\}$ kW/m^2
- Fig. 10.87 Starting and steady-state performances of I_{PV} , V_{PV} , I_{BES} , V_{BES} , v_g , i_g , v_L , i_L , ω_m under IDM at (a) 1kW/m^2 , and (b) 0.5kW/m^2
- Fig. 10.88 Dynamic performances of (a) G , V_{PV} , I_{PV} , P_{PV} , V_{BES} , I_{BES} , P_{BES} , and (b) v_g , i_g , v_L , i_L , i_{abcm} , ω_m , θ_e under IDM for change in irradiation from $\{1.0\text{-to-}0.5\}$ kW/m^2
- Fig. 10.89 Performances of (a) T_{syn} , θ_g , θ_L , e_θ , V_{pv} , u_p , and (b) v_g , i_g , v_L , i_L , v_{gp} for changeover from grid connected mode to islanded mode
- Fig. 10.90 Performances of (a) T_{syn} , θ_g , θ_L , e_θ , V_{pv} , u_p , and (b) v_g , i_g , v_L , i_L , v_{gp} for changeover from islanded mode to grid connected mode
- Fig. 10.91 MPPT performances of PV array at (a) 1.0kW/m^2 , and (b) 0.5kW/m^2
- Fig. 10.92 Steady-state performances under GCM at (a-c) 1kW/m^2 , and (d-f) 0.5kW/m^2
- Fig. 10.93 Dynamic performances of system under GCM for change in irradiation from (a-c) $\{1.0\text{-to-}0.5\}$ kW/m^2 , and (d-f) vice-versa
- Fig. 10.94 Steady-state performances under IDM at (a-c) 1kW/m^2 , and (d-f) 0.5kW/m^2
- Fig. 10.95 Dynamic performances of system under IDM for change in irradiation from (a-c) $\{1.0\text{-to-}0.5\}$ kW/m^2 , and (d-f) vice-versa
- Fig. 10.96 Performances of system for seamless mode transition from (a-d) GCM-to-IDM, and (e-h) IDM-to-GCM.

LIST OF TABLES

Table 2.1	Major Milestones in Development of Solar Technology
Table 2.2	Comparison Among Various Sensorless Techniques
Table 3.1	Rated Parameters of RS-PMSM
Table 3.2	Non-Oriented Silicon Steel Specifications
Table 3.3	Key Dimensions of Presented RS-PMSM
Table 3.4	Experimental and FEA Results of RS-PMSM
Table 4.1	Ratings of Designed RS-PMSM-WMB
Table 4.2	Design Variables of RS-PMSM-WMB
Table 4.3	Parameters of RS-PMSM-WMB For Top Five Design Sets
Table 4.4	Initial and Optimized Parameters of the RS-PMSM-WMB
Table 4.5	Detailed Parameters of the Designed RS-PMSM-WMB
Table 4.6	Main Parameters of Presented RS-PMSM-WPB
Table 4.7	Variation range of barrier dimensions
Table 4.8	Selected Flux-Barrier Dimensions
Table 4.9	Comparison Between RS-PMSM-WMB and CS-PMSM
Table 5.1	List of main System Components

LIST OF ABBREVIATIONS

AC	Alternating Current
ADC	Analog to Digital Converter
ANF	Adaptive Notch Filter
AMNF	Adaptive Multi-Notch Filter
APF	All Pass Filter
ASTM	American Society for Testing and Materials
BDC	Bidirectional Converter
BIS	Bureau of Indian Standards
BJT	Bipolar Junction Transistor
BLDCM	Brushless DC Motor
BES	Battery Energy Storage
CCM	Continuous Conduction Mode
CEC	Clean Energy Council
CER	Clean Energy Regulator
CPU	Central Processing Unit
CS-PMSM	Conventional Spoke PMSM
DAC	Digital to Analog Converter
DC	Direct Current
DSC	Delayed Signal Cancellation
DSO	Digital Signal Oscilloscope
DSP	Digital Signal Processor
DTC	Direct Torque Control
EMC	Electro-Magnetic Compatibility
EMF	Electro-Motive Force
EMI	Electro-Magnetic Interference
EMN	Electromagnetic Noise
FEA	Finite Element Analysis
FEC	Front End Converter

FEM	Finite Element Method
FL	Fuzzy Logic
FLL	Frequency Locked Loop
FOC	Field Oriented Control
GCC	Grey Correlation Coefficient
GCG	Grey Correlation Grade
IB	Internal Barriers
IEC	International Electrotechnical Commission
IEEE	Institute of Electrical and Electronics Engineers
IANF	Improved Adaptive Notch Filter
IGBT	Insulated Gate Bipolar Junction Transistor
INC	Incremental Conductance
ISES	International Solar Energy Society
IM	Induction Motor
INC	Incremental Conductance
IS	Indian Standard
ISOGI	Improved SOGI
KF	Kalman Filter
LPF	Low Pass Filter
MAF	Moving Average Filter
MMF	Magnetomotive Forces
MPP	Maximum Power Point
MPPT	Maximum Power Point Tracking
NdFeB	Neodymium-Iron-Boron
PB	Peripheral Barriers
PFC	Power Factor Correction
PI	Proportional Integral
PLL	Phase Locked Loop
PMBDCM	Permanent Magnet Brushed DC Motor
PMD	Permanent Magnet Demagnetization

PM	Permanent Magnet
PMSM	Permanent Magnet Synchronous Motor
PQ	Power Quality
P&O	Perturb and Observe
PV	Photo-Voltaic
PWM	Pulse Width Modulation
RE	Renewable Energy
RMS	Root Mean Square
RS-PMSM	Reverse Saliency PMSM
RS-PMSM-WMB	Reverse Saliency PMSM With Multilayer Barriers
RS-PMSM-WPB	Reverse Saliency PMSM With Peripheral Barriers
SHE	Selective Harmonic Elimination
SMO	Sliding Mode Observer
SOGI	Second Order Generalized Integrator
SMPS	Switched Mode Power Supply
SRF	Synchronous Reference Frame
SRM	Switched Reluctance Motor
STC	Standard Test Condition
SWPS	Solar Water Pumping System
SyRM	Synchronous Reluctance Motor
TF	Transfer Function
THD	Total Harmonic Distortion
UPF	Unity Power Factor
UVT	Unit Vector Template
VSC	Voltage Source Converter
VSI	Voltage Source Inverter
WPS	Water Pumping System

LIST OF SYMBOLS

AH_{BES}	Ampere-hour capacity of BES
AH_{BESn}	Nominal ampere-hour capacity of BES
EC_{BES}	Energy capacity of BES
EC_{BESn}	Nominal energy capacity of BES
C_f, r_f	Capacitor, and resistor across RC-ripple filter
C_{DC}	Capacitor across DC bus
C_{PV}	PV array capacitor
D	Duty ratio of boost converter
DOD	BES Depth of Discharge
e_α, e_β	$\alpha\beta$ -axis back EMF components
e_ω	Speed error
e_{vdc}	DC link voltage error
f_{sb}	Switching frequency of boost converter IGBT
G	Solar irradiation
I_d, I_q	dq-axes currents of PMSM
I_{dr}, I_{qr}	Reference dq-axes currents of PMSM
i_α, i_β	$\alpha\beta$ -axes PMSM currents
i_{ga}, i_{gb}, i_{gc}	Grid currents
i_{gr}	Reference grid currents
i_{ma}, i_{mb}, i_{mc}	PMSM currents
$i_{mar}, i_{mbr}, i_{mcr}$	Reference PMSM currents
I_{dm}, I_{qm}	dq-components of the PMSM currents
I_{dmr}, I_{qmr}	Reference dq-components of the PMSM currents
$I_{PVr}, V_{PVr}, P_{PVr}$	Reference value of PV array current, voltage, and power
I_{PV}, V_{PV}, P_{PV}	PV array current, voltage, and power at MPPT
I_{sc}, V_{oc}	PV array short circuit current and open circuit voltage
$I_{BES}, V_{BES}, P_{BES}$	BES current, voltage, and power
$I_{BESn}, V_{BESn}, P_{BESn}$	Nominal BES current, voltage, and power

i_L, v_L	Load current, and load voltage
i_{Lin}, i_{Lq}	In-phase and quadrature component of load current
i_{Lf}	Filtered load current
i_{Lfr}	Reference value of filtered load current
v_{Lr}	Reference load-voltage
I_{BESr}	Reference BES current
I_{DC}	DC link current
L	Inductance of boost converter
L_f	Inductance of interfacing inductor
N_r	Rated speed of PMSM
N_p	Number of poles in PMSM
P_L	Active power requirement of load
P_{pmsmr}	Rated power of PMSM
P_{pmsm}	Output power of PMSM
Q_L	Reactive power requirement of load
S_L	Apparent power requirement of load
T_{b1}, T_{b2}	Switching pulses for bidirectional converter
$T_{m1}-T_{m6}$	Switching pulses for motor-side three-phase VSI
$T_{g1}-T_{g6}$	Switching pulses for grid-side three-phase VSC
$T_{g1}-T_{g4}$	Switching pulses for grid-side single-phase VSC
T_{em}, T_{mech}	Electromagnetic and mechanical PMSM torque
T_{est}	Estimated PMSM torque
T_{ref}	Reference PMSM torque
T_L	Load torque
T_{syn}	Status of synchronizing switch
u_{gp}	Unit template corresponding to grid voltage
v_{α}, v_{β}	$\alpha\beta$ -axes PMSM voltages
V_{DC}	DC link voltage
V_{DCr}	Reference DC link voltage
V_{Lp}	Peak value of load voltage

v_{ag}, v_{bg}, v_{cg}	Estimated grid voltages per phase
$v_{abg}, v_{bcg}, v_{cag}$	Estimated line-to-line grid voltages
V_{rmsg}	RMS grid voltage
v_{ma}, v_{mb}, v_{mc}	PMSM phase-voltages
$v_{mab}, v_{mbc}, v_{mca}$	PMSM line-voltages
w_T	Total weighting-component
w_{loss}	DC-loss weighting factor
w_L	Load weighting-factor
$\lambda_{\alpha}, \lambda_{\beta}, \lambda_r$	$\alpha\beta$ -axes and resultant PMSM flux
ϕ_{pm}	Permanent magnet flux linkage
θ_{me}	Estimated rotor angle
θ_g	Phase-angle of grid voltage
θ_L	Phase-angle of load-voltage
ω_e	Estimated PMSM speed in elect.
ω_g	Grid frequency
ω_{me}	Estimated PMSM speed in mech.
ω_{mrt}	Rated PMSM speed
ω_{mer}	Reference PMSM speed in elect.